Beach Evolution Adjacent to a Seasonally Varying Tidal Inlet in Central Vietnam

Authors: Do, Anh T.K., de Vries, Sierd, and Stive, Marcel J.F.

Source: Journal of Coastal Research, 34(1) : 6-25

Published By: Coastal Education and Research Foundation

URL: https://doi.org/10.2112/JCOASTRES-D-16-00208.1

Journal of Coastal Research	34	1	6–25	Coconut Creek, Florida	January 2018

Beach Evolution Adjacent to a Seasonally Varying Tidal Inlet in Central Vietnam

Anh T.K. Do[†‡]*, Sierd de Vries[†], and Marcel J.F. Stive[†]

[†]Faculty of Civil Engineering and Geosciences
Delft University of Technology
Delft, The Netherlands

[‡]Faculty of Water Resources Engineering
University of Da Nang (UD)–University of Science and Technology (DUT)
Da Nang, Viet Nam

www.cerf-jcr.org

www.JCRonline.org

ABSTRACT

Do, T.K.A.; de Vries, S., and Stive, M.J.F., 2018. Beach evolution adjacent to a seasonally varying tidal inlet in central Vietnam. *Journal of Coastal Research,* 34(1), 6–25. Coconut Creek (Florida), ISSN 0749-0208.

Cua Dai Inlet is a typical, seasonally varying tidal inlet in central Vietnam. Since 1995 the northern adjacent coast, known as Cua Dai Beach, has experienced serious erosion. The decadal scale behavior of this inlet appears to reflect a nonperiodic cyclic process. Inlet channel shifting from north to south has welded the abandoned ebb-tidal delta with Cua Dai Beach, leading to accretion but subsequently triggering erosion. Although erosion of Cua Dai Beach was exacerbated by decrease of sediment supply from the estuary and ebb-tidal delta and by coastal developments, the channel shifting to the south, and the ebb shoal development were important primary controlling mechanisms. This study aims to quantify the main erosional processes in and near the Cua Dai coastal inlet and adjacent beaches since 1995. First, satellite data were used to detect shoreline change trends and to estimate volume changes. Second, alongshore, wave-driven sediment transports were estimated using numerical models. Observed shoreline changes indicate that, during the period from 2000 to 2010, erosion rates at the northern side of the inlet were on average 12 m/y. Close to the inlet, erosion rates were larger, up to 19 m/y. At the same time, the southern coast of the inlet was found to accrete with a mean rate of 11 m/y. Calculated alongshore sediment transport rates explain the observed erosion and accretion patterns. The overall system lost a significant sediment volume, which is estimated to amount to 243,000–310,000 m^3/y. A logical conclusion is that the effects of the shifting of the inlet channel to the south caused erosion of the northern adjacent coast, whereas human interventions in the river catchment, the estuary, and along the coast contributed importantly to the overall sediment deficit of the inlet system and its beaches and to the shifting erosion pattern toward the north.

ADDITIONAL INDEX WORDS: *Shoreline change, Cua Dai, sediment budget, longshore transport, inlet channel shifting, bar welding*.

INTRODUCTION

Tidal inlets connecting an estuary, lagoon, or river to the coast are commonly found throughout the world (Elias and van de Spek, 2006; Kragtwijk *et al*., 2004; Oertel, 1988; Stive and Wang, 2003). Tidal inlets showing seasonal behavior are found at many locations in Southeast Asia and Australia because of variability in monsoon wind directions or dry and wet periods (Duong *et al*., 2016; Stive, Tran, and Nghiem, 2012). Coastal features near inlets are generally amongst the most dynamic regions (Stive *et al*., 2009). They are not only affected by ocean processes (tides, waves, and mean sea level), but also by fluvial and estuarine processes (Duong *et al*., 2016; Lam, 2009; Ranasinghe *et al*., 2013; Tung, 2011). Furthermore, they are increasingly influenced by human interventions such as dredging, coastal structures, and land reclamation in the tidal basins. The complex feedbacks between the forcing and response of inlet systems influenced by variations in a seasonal wave climate combined with human interventions have received a broad scientific interest (Dissanayake, Ranasinghe, and Roelvink, 2012; Lam, 2009; Ranasinghe, Pattiaratchi, and Masselink, 1999; Stive, 2004; Tung, 2011).

In central Vietnam, one finds many seasonally varying tidal inlets. These inlets are in a microtidal, wave-dominated, coastal environment and experience a strong seasonal variation in river discharge and wave climate (Ranasinghe and Pattiaratchi, 1999; Tung, 2011). The climate in central Vietnam is strongly governed by tropical monsoons. Two main seasons can be distinguished, the dry or summer season and rain or winter season.

Cua Dai Estuary in central Vietnam is a typical, seasonally varying inlet connected to the catchment area of the Vu Gia and Thu Bon rivers. The total catchment area is approximately 10,350 km^2 and includes roughly 90% of the Quang Nam Province and 10% of Danang City. The catchment area of the Thu Bon Basin is 4100 km^2 at the Cua Dai Inlet. The total length of the main river is 152 km. Between the Vu Gia River and the Thu Bon River, there are two connecting tributaries, Quang Hue and Vinh Dien (see Figure 1). Because of the exchange of their discharges, these two rivers need to be considered as one river basin system. Figure 1 shows a map of the river network and of the location of hydrometeorological stations as well as of hydropower plants. Another distinctive feature in this system is the Cham Islands group, which is comprised of a group of eight islands, located about 16 km in the NE direction from the Cua Dai Inlet. Besides natural processes, this system has been influenced by human activity. The human activities are the construction of hydropower plants upstream of the Vu Gia–Thu Bon Basin, the construction of resorts near

DOI: 10.2112/JCOASTRES-D-16-00208.1 received 19 November 2016; accepted in revision 21 February 2017; corrected proofs received 30 May 2017; published pre-print online 28 July 2017.
*Corresponding author: T.K.A.Do@tudelft.nl

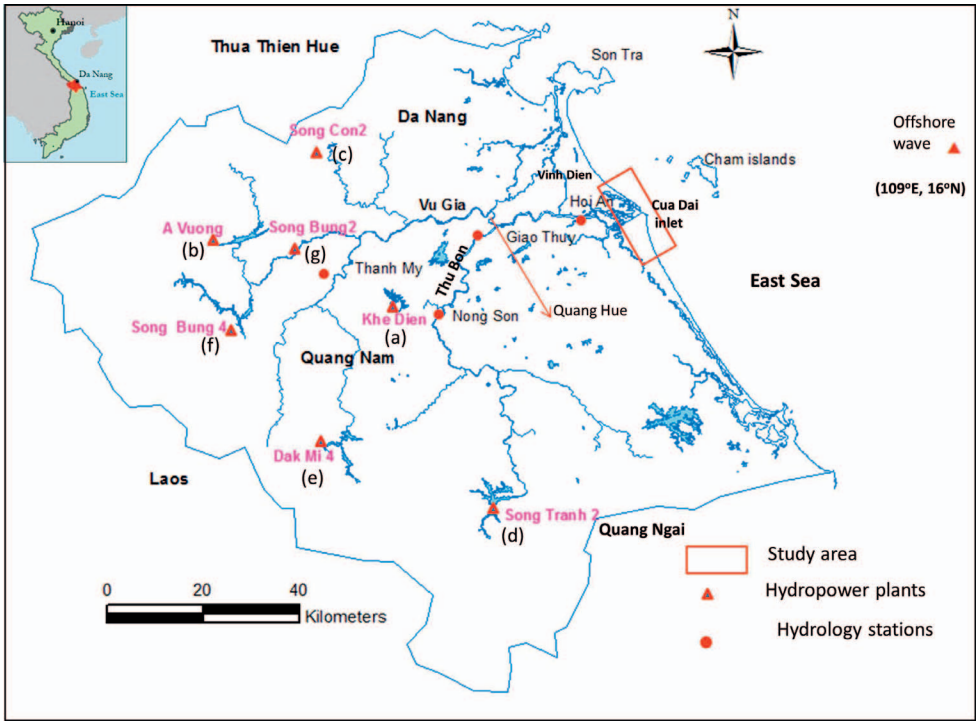

Figure 1. Location of Cua Dai Inlet and the Vu Gia–Thu Bon River system.

and on the beach, land reclamations, and sand mining for building and infrastructure in the estuary (Tuoitre, 2015).

Since 1995, Cua Dai Beach, located on the north side of Cua Dai Inlet, has experienced severe erosion (Vnexpress, 2014, 2015). The long-term geomorphological development of this inlet appears to reflect a nonperiodic process of cyclic channel switching that takes place over several decades. In addition, coastal developments leading to squeeze and decrease of sediment supply from the river and the estuary took place. These factors have created changes in sediment budgets and have put Cua Dai Beach under stress by causing the shoreline to erode. This study aims to quantify the erosion processes in the Cua Dai coastal inlet and adjacent beach system since 1995. To aid future management of this system, it is necessary to understand the factors that influence the existing morphology and that cause coastal retreat of the system. Insight into the effects and causes of these changes can be gained by reconstructing historical shoreline positions in combination with process-based modelling to understand longshore sediment transport patterns and associated sediment budget changes over recent decades under the impact of human interventions.

Environmental Conditions

Both the river flow regimes and coastal processes such as waves and tides influence Cua Dai Inlet and its adjacent coasts. The tide range is 0.7 m (Lam, 2009; Tung, 2011) and the wave height ranges from 0 to 2 m. Therefore, Cua Dai is classified as a microtidal, mixed-energy/wave-dominated inlet according to Hayes' (1979) tidal classification diagram.

The monsoon influences both the wave conditions and the river flow. During the NE monsoon regime, waves in the winter season (from September to March) are mainly from the ENE direction. In the summer months (from April to August) when the SW monsoon is active, waves come from the SE and ENE. In terms of river discharge, previous studies (Ho, Umitsu, and Yamaguchi, 2010; Lam, 2009; Tung, 2011) show that there are two distinctive seasons, a flood season lasting from September to December and a dry season lasting from January to August.

When combining both the hydrology and the wave climate, we may conclude that three seasons exist, an ENE monsoon with a flood season from September to December, an ENE monsoon with a dry season from January to March, and a dry bidirectional SE/ENE monsoon from April to August. The winter/flood season lasts for 4 months, from September to December, with an average discharge of 625 m^3/s. The average discharge during the winter/dry season, from January to March, is 160 m^3/s, whereas the average discharge during the summer/dry season is only 88 m^3/s. Figure 2 also indicates that the high values of monthly discharge at the Nong Son Station often occur in 3 months: October, November, and December. During the relatively long dry period the flow is quite low, with a lowest average discharge of 71 m^3/s in July. The average annual discharge from 1977 to 2011 at the Nong Son Station is 285 m^3/s.

In recent years, floods occur more frequently and with higher peak discharges. The highest discharge that occurred every year from 1977 to 2011 is displayed in Figure 3. The red points indicate the average of the yearly highest discharges over the

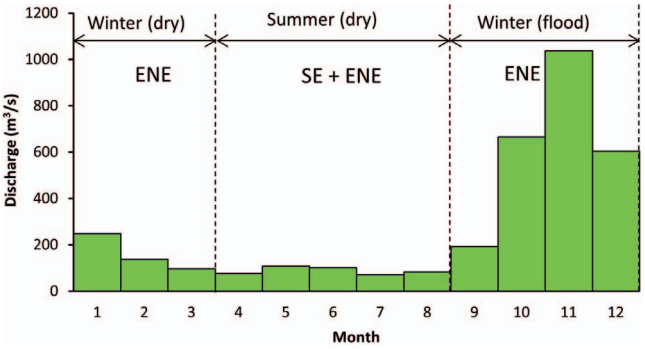

Figure 2. Seasonal variation of the average monthly discharge at Nong Son Station, upstream the Thu Bon River (1977–2011). ENE and SE are the dominant wave directions in each season.

preceding 10-year period. The trends indicate an increase in the 10-year mean highest discharges. The reason behind this is unknown. Extreme floods occurred in 1986, 1998, 1999, 2007, 2009, and 2011. The floods were often induced by intense meteorological phenomena (heavy rain, storm, typhoon, or tropical depression). These events caused severe damage in terms of loss of life and infrastructure. The green bars in Figure 4 present the number of floods that occurred every year from 1989 to 2010 (data by the Asian Development Bank, 2014). For the number of floods in recent years from 2011 to 2015, we lack this information. This figure indicates that during recent years, from 2005 to 2010, floods occur more frequently. In 2005, six floods occurred. In 2007 nine floods occurred, of which one was an extreme flood with a peak discharge of 10,600 m^3/s. In general, the average number of floods that occurred during 2005 to 2010 is 5.6 floods per year, whereas the average number of floods during the period from 1989 to 2004 is only 2.7 floods per year. These data indicate that also the number of floods has increased in recent years at the Vu Gia–Thu Bon Basin.

Besides the increasing frequency and increasing magnitude of river floods, the Quang Nam Province experiences storms, typhoons, tropical depressions, and human interventions. An overview of the most important events and human interventions is shown in the time line in Figure 4. The data of storms, typhoons, and tropical depressions were extracted from the National Weather Service (United States) by using individual storm-tracking records at location 15° N, 110° E in the western Pacific. The classification of hurricanes based on the Saffir/Simpson hurricane scale is used, which defines a tropical depression as having wind speed less than 34 knots, a tropical storm with wind speed from 34 to 63 knots, and a hurricane or typhoon with wind speeds greater than 64 knots. In general, 68 tropical cyclones and depressions occurred that affected or directly hit the coastline of the Quang Nam Province during the period from 1988 to 2014, with an average of 2.5 cyclones per year. This includes 27 typhoons, 24 tropical storms, and 17 tropical depressions. There were four big typhoons that hit directly, causing heavy rain and subsequent flooding. These were Typhoon Cecil (May 1989), Typhoon Xangsane (October 2006), Typhoon Ketsana (September 2009), and Typhoon Nari (October 2013).

Since 2000 there have been many human activities such as the building of resorts at Cua Dai Beach, the construction of hydropower plants upstream, and land reclamations inside the estuary for urbanization purposes. The date of the construction of the resorts and hydropower plants as well as land

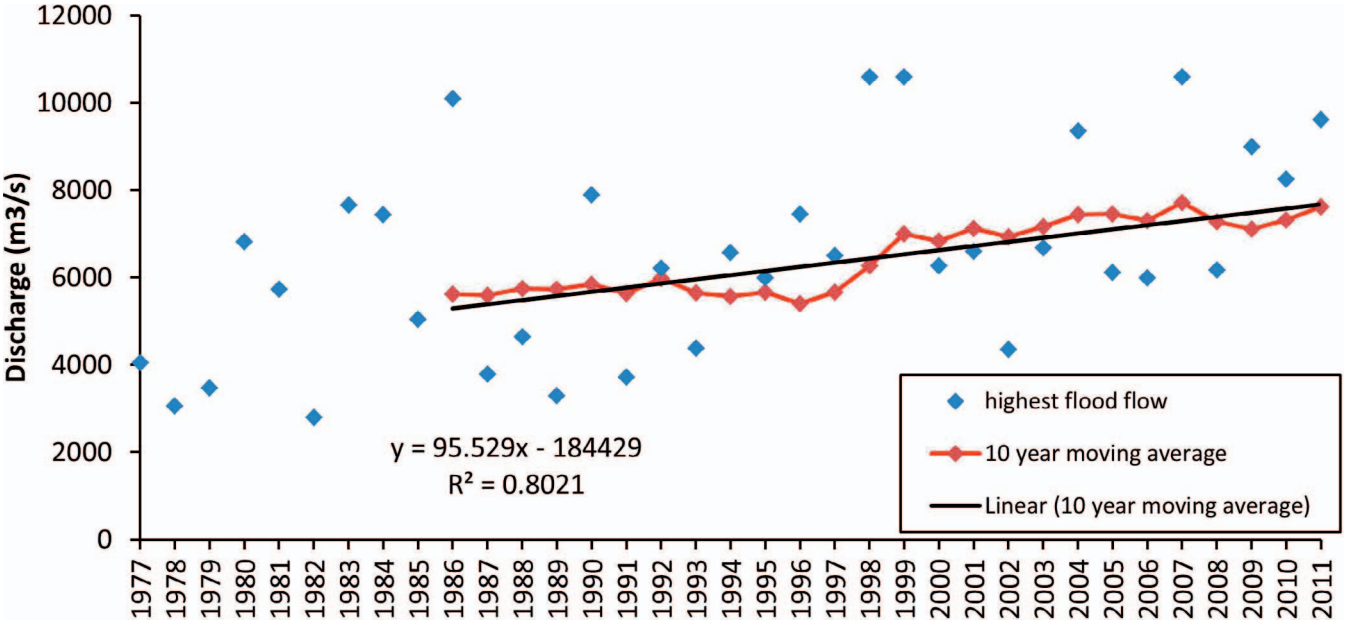

Figure 3. Yearly highest flood discharge at Nong Son Station (1977–2011). The black line indicates the mean of the yearly highest flood discharge over the preceding 10-y period.

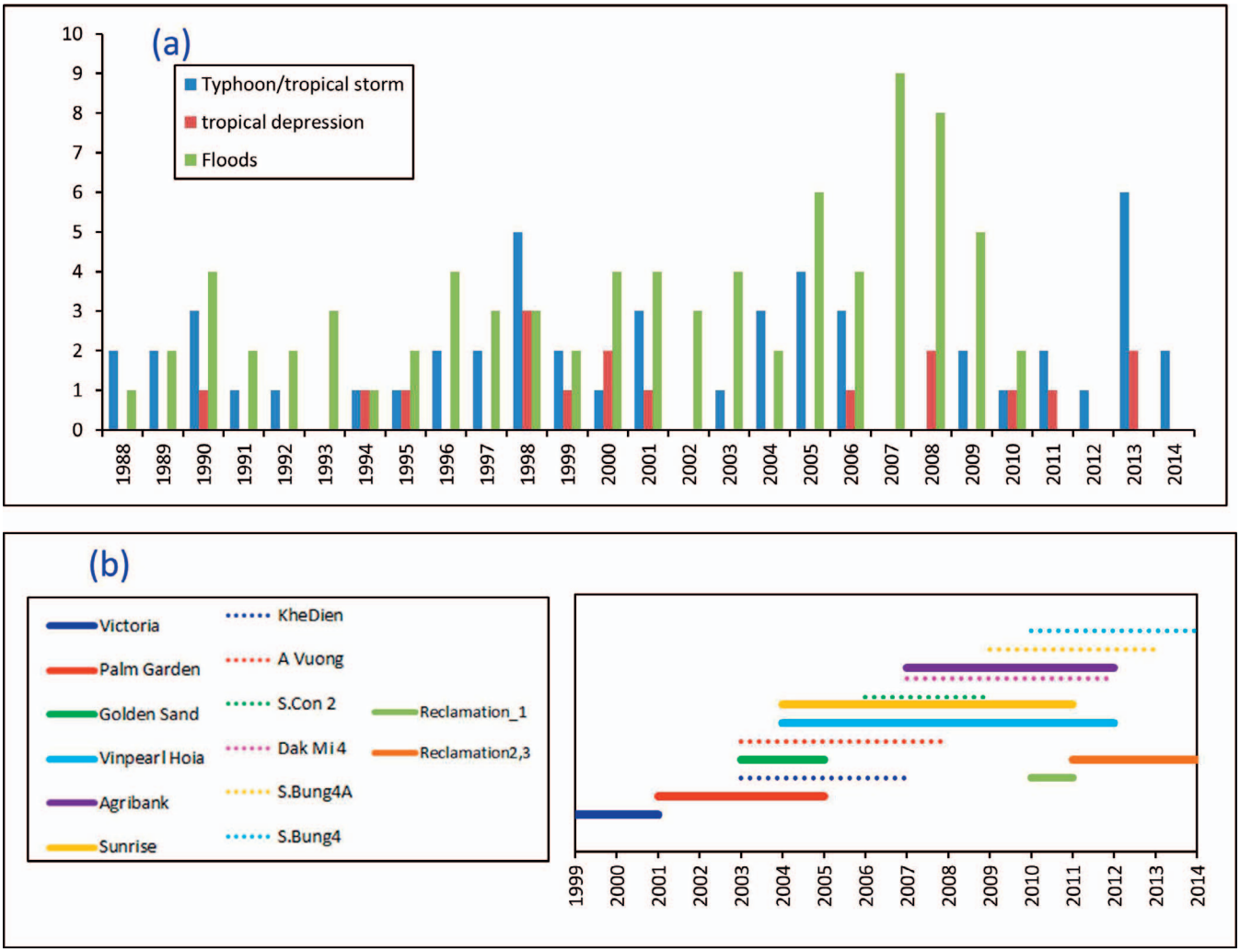

Figure 4. Time line of events and human interventions at the Vu Gia–Thu Bon River basin. (a) The number of typhoons/tropical storms, tropical depressions, and floods (note that from 2011 to 2014 no data on floods are available); (b) construction period of resorts, hydropower plants, and reclamations (solid lines indicate the name of resorts, whereas dotted lines indicate the name of hydropower plants).

reclamations were derived from observations based on a series of Landsat images and local papers (A Vuong Joint Stock Hydropower Company, 2011; Song Ba Joint Stock Company, 2015; Song Bung 4 Hydropower Project Management, 2015). The location of the hydropower plants is indicated in Figure 1 and the location of the resorts and land reclamations in Figure 5. Starting from Cua Dai Inlet and going along the beach toward the north, the first resort is Vinpearl Hoi An. The construction started around 2004. After the construction, the shoreline significantly retreated so that the investors chose to protect their resort by construction of a seawall in front of the resort. The second resort is Fusion Alya, which was constructed during the period 2010 to 2012. This resort also has a seawall to protect itself from severe erosion. A 700-m stretch between Fusion Alya and Sunrise Resort has been protected by a heavy embankment along this stretch funded by the Ministry of Construction, which presently has toe erosion. Groynes made of large geobags defend the third resort, Sunrise, constructed in the period 2006 to 2011. The fourth resort, Golden Sand, constructed from 2002 to 2005, has been protected by a riprap stone embankment. The last one in this row of five is Victoria Resort, the first resort that was constructed at Cua Dai Beach in 1999. Presently, it also uses a stone riprap embankment to protect against erosion. Farther to the north there are two more resorts, Agribank and Palm Garden. These were less affected by shoreline retreat, but very recently in October 2016 erosion has reached this location as well (M.J.F. Stive, *personal observation*).

METHODS

To investigate the erosion at Cua Dai Beach, the present work collected the available data concerning its past evolution. Satellite data and GIS techniques were used to estimate the trends in shoreline evolution and volume changes during

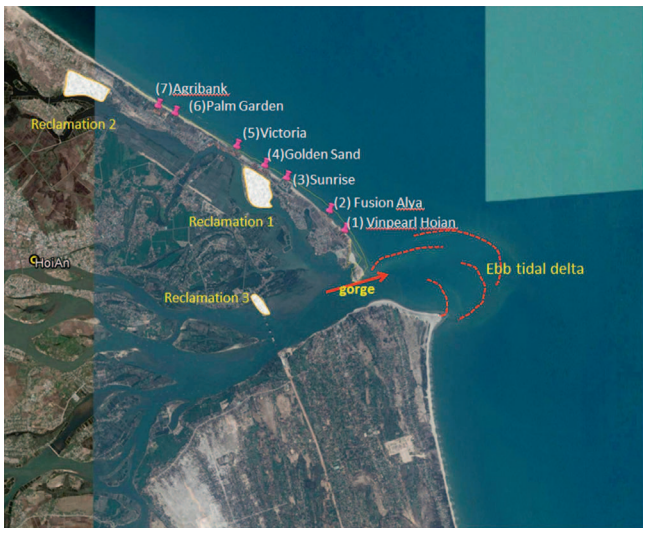

Figure 5. Location of resorts and land reclamations and the ebb-tidal delta of Cua Dai Beach.

recent decades. The numerical model Simulating WAves Nearshore (SWAN) combined with an empirical equation was applied to calculate the local longshore sediment transport rate (LSTR) and the gradients in LSTR. On the basis of the results of the LSTR and shoreline change rate as well as the background information of Cua Dai Beach, this study aims to explain the prevailing transport mechanisms and especially those causing erosion problems in this system.

Rates of Change in Shoreline Location

Recent progress in remote sensing and GIS techniques has been proposed as a relatively low-cost approach to coastal monitoring (Maiti and Bhattacharya, 2009). Many applications of remote sensing and GIS on mapping shorelines and inlet dynamics demonstrate that satellite-based remote sensing can be a useful tool for mapping shoreline changes and the dynamic behavior of tidal inlets, rivers, and estuaries (Avinash, Deepika, and Jayappa, 2013; Avinash, Jayappa, and Vethamony, 2012; Chen and Chang, 2009; Gilvear, Tyler, and Davids, 2004; Panda, Mohanty, and Samal, 2013; Pari *et al*., 2008; Rajawat *et al*., 2007; Ryu *et al*., 2008).

To detect the shoreline location in Cua Dai Beach during the last decades, a total of six multispectral satellite images acquired on different dates were selected on the basis of the lowest cloud cover (Table 1). The six orthorectified satellite images of the study area from the sensors Landsat-5TM, Landsat-7 ETM+, and Landsat-8 OLI-TIRS in the years, 1988, 1995, 2000, 2005, 2010, and 2015 were downloaded from U.S. Geological Survey (USGS) Earth Explorer web tool. The images in the years between 1990 and 1995 were not selected because of the poor quality. Although the image of 2005 was selected to extract the shoreline position, it was eventually not used to present these shoreline change results, since the trends from 2000 to 2005 and from 2005 to 2010 are very similar.

The methodology to extract the shoreline includes three steps: (1) conversion of the digital number to spectral radiance and to the top of atmospheric (TOA) reflectance for radiometric calibration according to Chander, Markham, and Helder (2009); (2) application of the normalized difference water index (NDWI) (McFeeters, 1996) to enhance the TOA reflectance; and (3) delineation of the land–sea boundary was achieved using isocluster unsupervised classification and the enhanced NDWI images. Then, the boundary between land and sea in the classified image is converted into a vector file for shorelines in ArcGIS software.

The shoreline change rates are estimated for four zones around Cua Dai Inlet: zone A (northern coast), zone B (southern coast), zone C (riverbank), and zone D (extent of spit due to welding of tidal bar). Transects were chosen at simple right angles from the baseline at 50-m intervals (Figure 6). Zone A includes 74 transects (3650 m) from transect A1 to transect A74 starting from the north. Zone B also includes 74 transects from transect B1 to transect B74 (3650 m). The riverbank, zone C, includes 49 transects (2400 m) from C1 to C48, starting from the river toward the sea.

Shoreline change rates are calculated following the end point rate (EPR) method using the digital shoreline analysis system (DSAS) software version 4.3, an ArcGIS extension for calculating shoreline change developed by the USGS (Thieler *et al*., 2009). The EPR is calculated by dividing the distance of shoreline movement by the time elapsed between the earliest and latest measurements at each transect (Thieler *et al*., 2005, 2009). A baseline is constructed to serve as a starting point for all transects derived by the DSAS application. Using the EPR method, shoreline change rates in each period between 1988 and 1995, 1995 and 2000, 2000 and 2010, and 2010 and 2015 are calculated. Shoreline change rate at every transect location is calculated by subtracting two derived shoreline locations at the beginning and the end of each period.

Calculation of Volume Changes

To understand sediment sources, sinks, and transport pathways in a coastal system, the concept of estimating a sediment budget is commonly used (Hapke *et al*., 2010; Rodríguez and Dean, 2009; Rosati, 2005). This study uses the satellite-derived shoreline change rates to calculate the volume changes ΔV (m^3/y) for each zone A, B, C, and D. The cell volume

Table 1. *Characteristics of images analyzed.*

Name	Acquisition Date	Path/Row	Resolution (m)	Type	Used Bands
Landsat 5 TM	3 September 1988	124/049	30	Geo Tiff	2 and 4
Landsat 5 TM	19 June 1995	124/049	30	Geo Tiff	2 and 4
Landsat 7 ETM+	5 July 2000	124/049	30	Geo Tiff	2 and 4
Landsat 5 TM	16 July 2005	124/049	30	Geo Tiff	2 and 4
Landsat 5 TM	12 June 2010	124/049	30	Geo Tiff	2 and 4
Landsat 8 OLI-TIRS	10 June 2015	124/049	30	Geo Tiff	3 and 5

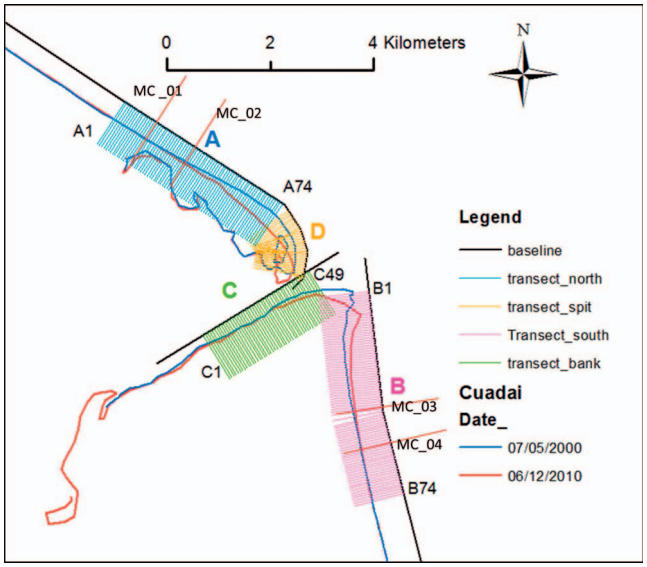

Figure 6. Transects at the northern side, the southern side, the riverbank, and the spit created with a 50-m interval to extract shoreline changes around Cua Dai Inlet.

changes (ΔV, m^3/y) were estimated by using Equation (1) (Rosati, 2005; Rosati and Kraus, 1999):

$$\Delta V = A_D \sum_{i=1}^{n} (\Delta y \Delta x) \quad (1)$$

where, Δy is the shoreline change rate for each transect (m/y), A_D is the average active depth for the cell (m), Δx represents the transect spacing (m), and n is the total transects of each zone. The active depth represents the vertical extent of the beach profile that is eroding or accreting during the period of consideration, and is typically defined as the absolute sum of the berm crest or dune elevation, B, and depth of closure, D_c (Equation [2]). However, in the absence of dune elevation data, it was assumed that the closure depth was representative for the active depth:

$$A_D = B + D_c \quad (2)$$

in which, B is assumed zero.

The depth of closure indicates the seaward limit of appreciable depth change or limit of longshore and cross-shore sediment movement (Hallermeier, 1978, 1981; Nicholls, Birkemeier, and Hallermeier, 1996; Rodríguez and Dean, 2009). In cases with no available data, an analytical approach is commonly used to estimate an annual depth of closure. Since no systematic measurements of the active beach profiles are available, this study used the method proposed by Hallermeier (1981) to estimate closure depth according to:

$$d_{l,t} = 2.28H_{e,t} - 68.5(H_{e,t}^2/gT_{e,t}^2) \quad (3)$$

where, $d_{l,t}$ is the predicted depth of closure over t years, related to mean low water; $H_{e,t}$ is the nonbreaking significant wave height that is exceeded 12 hours per t years; $T_{e,t}$ is the associated wave period; g is the acceleration due to gravity. The computed closure depth ($d_{l,t}$) by Equation (3) is verified to some extent by using two available bathymetric maps of the area from 2009 and 2010.

The wave characteristics used to compute closure depth were derived using nearshore wave models. Because the contour bathymetry is only available for 2 years (2009 and 2010), this study used wave conditions during this period to estimate the closure depth. First, the offshore wave conditions during 2009 and 2010 were extracted from the National Oceanic and Atmospheric Administration (NOAA) Wave Watch III archives at grid point (16.0° N, 109.0° E) (Figure 1), approximately 65 km offshore of Cua Dai Inlet. Then, SWAN transformed the extreme wave height that exceeds 12 hours in 2 years to the nearshore. The significant wave height and wave period in the nearshore were used in Equation (3) to estimate the annual closure depth. The results of this estimated closure depth are compared with the depth profiles available for 2009 and 2010. The results of estimated closure depth by Hallermeier (1981) are 5.2 to 6.3 m, corresponding to the nearshore significant wave height around Cua Dai Inlet of 2.8 to 3.3 m. The four profiles, MC_01, MC_02, MC_03, and MC_04 (Figure 6), in which two profiles located 4 km and 3.2 km north of Cua Dai Inlet and the other two profiles located 3.3 km and 2.6 km south of Cua Dai Inlet, indicate that the closure depth is around 6 to 7 m. To capture both ranges in values, the depth of closure for the study area is assumed to be from 5.5 to 7 m to calculate the shoreline volume changes.

Longshore Sediment Transport Capacity

The LSTR is estimated on the basis of the widely used Coastal Engineering Research Center (CERC) (USACE, 1984) formulae. The CERC formulation can be summarized as wave-driven alongshore sediment transport (S [m^3/s]) being proportional to the longshore wave energy flux (Bosboom and Stive, 2015):

$$S = \frac{K}{16\left(\frac{\rho_s}{\rho} - 1\right)(1-p)} \sqrt{\frac{g}{\gamma}} \sin(2\phi_b) H_b^{2.5} \quad (4)$$

where, ρ is the density of water (kg/m^3); ρ_s is the density of sediment (kg/m^3); p is the porosity; g is the gravitational acceleration (m/s^2); H_b is the significant wave height at the breaker line (m); γ is the breaker index; ϕ_b is the wave angle at the breaker line between wave propagation direction and shore normal direction (°); K is an empirical coefficient. USACE (1984) recommends a value of K of 0.39 when the significant wave height H_s is used. However, a value of 0.2 has been used on sandy beaches (Bayram, Larson, and Hanson, 2007; Schoonees and Theron, 1996) and 0.054 for a gravel beach (Ruiz de Alegria-Arzaburu and Masselink, 2010). $K = 0.2$ is used in this study since Cua Dai is a sandy beach.

To obtain first-order longshore sediment transport estimates, the offshore wave climate is transformed to a nearshore wave climate at the location of initial wave breaking and used as input to the CERC formulation (Equation [4]). Seasonal representative offshore wave directions are selected as input for the wave generation and propagation model, SWAN. Then the nearshore breaking wave height was derived from the

offshore to nearshore wave transformation by the SWAN model. The shoreline orientation was read from satellite imagery. The breaking wave heights and their direction relative to the shoreline orientation were used to estimate LSTRs for the summer and the winter seasons and for the year average.

The wave characteristics required for the calculation of wave-induced longshore sediment transport have been estimated using the offshore wave climate in combination with a numerical model. The only continuous series of wave data available is measured at the Con Co Station, approximately 188 km northward of the present study zone. Close to Cua Dai Beach, visual observations are available but the record is short in time and not continuous. Since observations are so limited, this study uses offshore wave conditions extracted from the NOAA Wave Watch III archives at grid point (16.0° N, 109.0° E) (Figure 1), which is approximately 65 km offshore of Cua Dai Inlet.

RESULTS

This section first presents the results of the offshore wave climate. Second, this section presents and discusses the results of shoreline changes and volume changes during the period 1988 to 2015. Third, the results of longshore sediment transport are presented and discussed. The longshore sediment transport is separately derived for the winter and the summer periods before aggregating these results into a net, yearly averaged result. This provides valuable insight into the seasonal variation.

Wave Climate

The offshore wave data in the period 2005–13 indicate that the wave climate in this area is strongly influenced by the monsoon regime. Figure 7 shows strong variations in height, period, and directional distribution of the waves. Because of the NE monsoon regimes, the wave direction in the winter season (from September to March) is dominated by the NE (7.1%) and ENE (79.5%). Considering the incoming waves between 60° and 75°, most wave heights range between 1.0 and 3.0 m and periods between 8 and 10 seconds. In the summer months (April to August), the waves are characterized by a bidirectional configuration. The waves are clearly influenced by the SE and ENE directional component. The first dominant direction is from the SE (44.7%), including waves coming from between 135° and 150°, with wave heights of 0–1.0 m and periods of 4–6 seconds. The second dominant wave direction is ENE (34.9%), with typical wave heights of 0.5–1.0 m and periods of 6–10 seconds. The highest wave heights normally occur during winter months because of typhoons or tropical storms and may reach up to 4–7 m in N, NE, ENE, E, and ESE directions. In general, waves during the winter season have higher energy and longer periods than waves in the summer season.

Shoreline Changes and Changes in Sediment Volume

Shoreline changes and changes in sediment volume were estimated in each of four selected periods, *i.e.* 1988 to 1995, 1995 to 2000, 2000 to 2010, and 2010 to 2015. The selection was based on comparability of the change pattern. The extracted shoreline positions are shown in Figure 8. These results indicate that in 1988 an ebb-tidal bar of the inlet existed. This suggests that the system was rich in sediment. Because of a big tropical storm that made landfall in May 1989 (Typhoon Cecil), the ebb-tidal bar merged with Cua Dai Beach, north of the inlet. Since 1995, after the welding of the ebb-tidal bar, this beach has been eroding.

Period 1988–1995

The long-term geomorphological development of the inlet reflects a nonperiodic cyclic process that takes place over several decades. Channel shifting from north to south dictates the geomorphological development of Cua Dai Beach, and much less so for the reverse situation for the southern beach. The channel shifting to the south in 1989 that created the new ebb shoal development was an important controlling mechanism. The welding of this ebb-tidal bar over this 7-year period (1989–95) with Cua Dai Beach explains the large accretion that the northern coast has experienced. Landsat 5TM data taken from 1988 to 1995 (Figure 9) illustrate how the tidal bar welded to the northern coast and formed a new sand spit that developed seaward and extended southward. For this reason, the northern coast experienced much accretion in this period. The accretion of the shoreline of the southern coast can probably be explained by having benefitted from the bypassing of sediments due to waves, tide, and floods, and the southern-directed longshore transports.

The shoreline change rates in three zones (A, B, and C) for the period from 1988 to 1995 are shown in Figure 10. The shoreline change rate results show the welding of the subareal beach barrier being part of the ebb-tidal delta of Cua Dai Inlet. Figure 10 also shows accretion on both sides of the inlet. An average increase in the shoreline of 25 m/y is observed for this 7-year period over the 2.6 km north of Cua Dai Inlet. For the first 2.5 km south of the inlet, the shoreline accreted with an average of 11 m/y, followed by a stable trend without any significant changes. The results of the riverbank show a relatively stable trend.

The derived volume changes for the 7-year period from 1988 to 1995 are shown in Table 2, where overall accretion is strongly evident. In general, north of the inlet (zone A) the volume increased by approximately 378,000 m^3/y to 481,000 m^3/y, corresponding to an active depth A_D of 5.5 m and 7 m respectively. The southern segment is characterized by a total accumulation of 114,000 m^3/y to 145,000 m^3/y. The riverbank shows an average reduction in the volume of –10,000 m^3/y to –13,000 m^3/y. Overall, the system seemed to be rich in sediment, with a total gain in zone A, zone B, and zone C of 481,000m^3/y (corresponding to 5.5 m D_c), of which 378,000 m^3/y was due to the welding.

Period 1995–2000

The shoreline change rates from 1995 to 2000 are presented in Figure 11. For the 2550-m segment north of zone A, there is an average positive trend of 3 m/y. Then, from transect A53 to transect A74 (1100 m), the shoreline has eroded with a mean rate of erosion of 18 m/y. The beach immediately south of the inlet showed accretion with mean of 0.7 m/y from 1.0 km to 2.4 km, followed by an erosional segment of 2.6 m/y over a 1.9-km stretch of beach. It seems that no bypassing occurred during this period. The riverbank segment experienced strong erosion of its estuarine shoreline, with a mean rate of 25 m/y. The

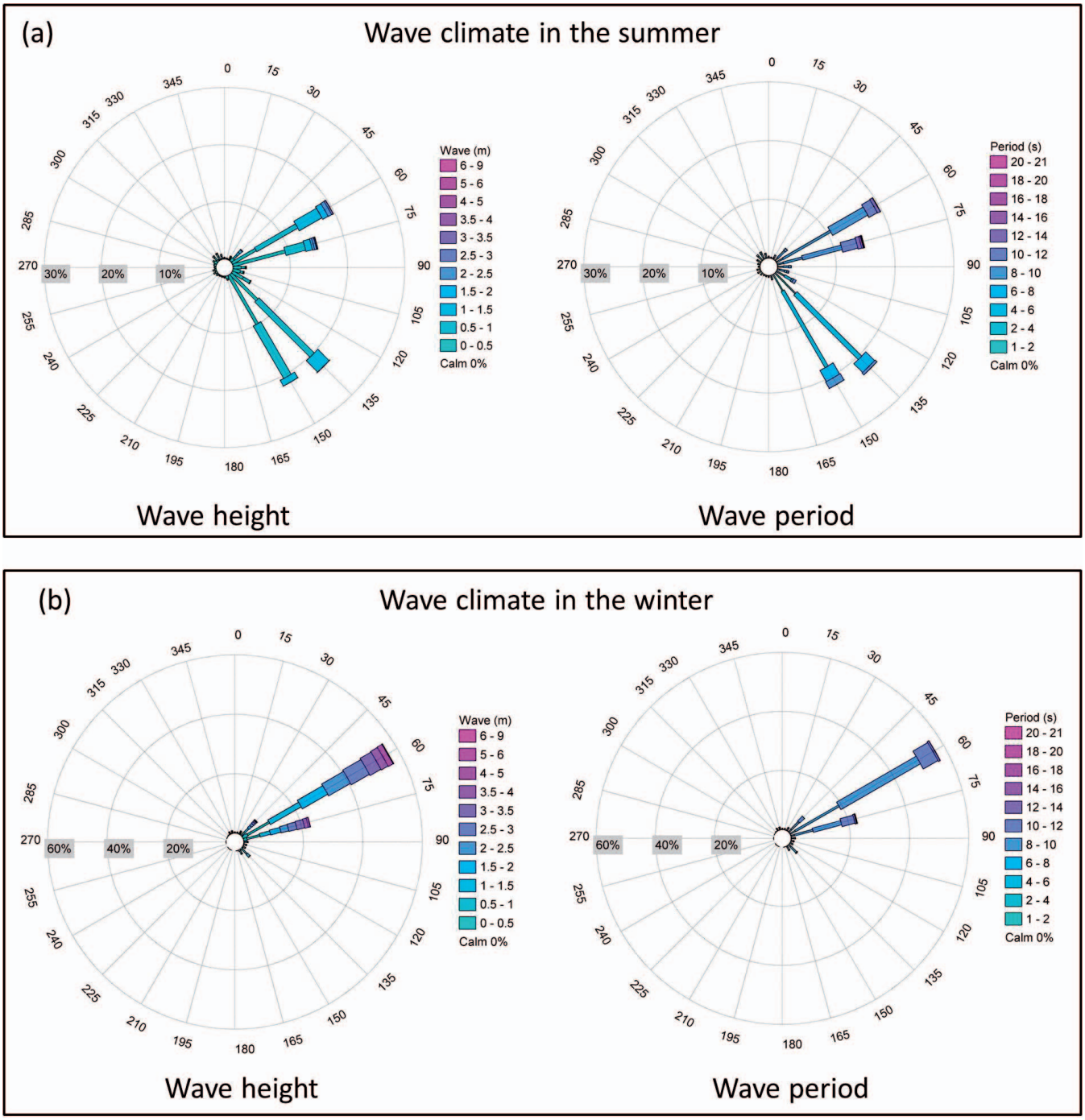

Figure 7. Occurrence frequencies for directional wave height and wave period. (a) Wave climate in the summer; (b) wave climate in the winter.

significant retreat of all three zones is possibly related to the completion of the welding of the beach barrier and due to extreme flood events in 1998 and 1999 (Figure 3).

The derived volume changes for the period of 1995 to 2000 are summarized in Table 2. A total of 60,000 m^3/y to 77,000 m^3/y has been lost at the north and 22,000 m^3/y to 29,000 m^3/y at the south. There was a large loss in sediment of the riverbank, with an average of 335,000 m^3/y to 426,000 m^3/y. The whole system lost 418,000 m^3/y, of which the riverbank lost 335,000 m^3/y. The big erosion that occurred at the riverbank might be related to the two extreme floods in 1998 and 1999 (Figure 3). These floods may have scoured the riverbank and flushed sediment into the ebb-tidal delta and later feeding zone B.

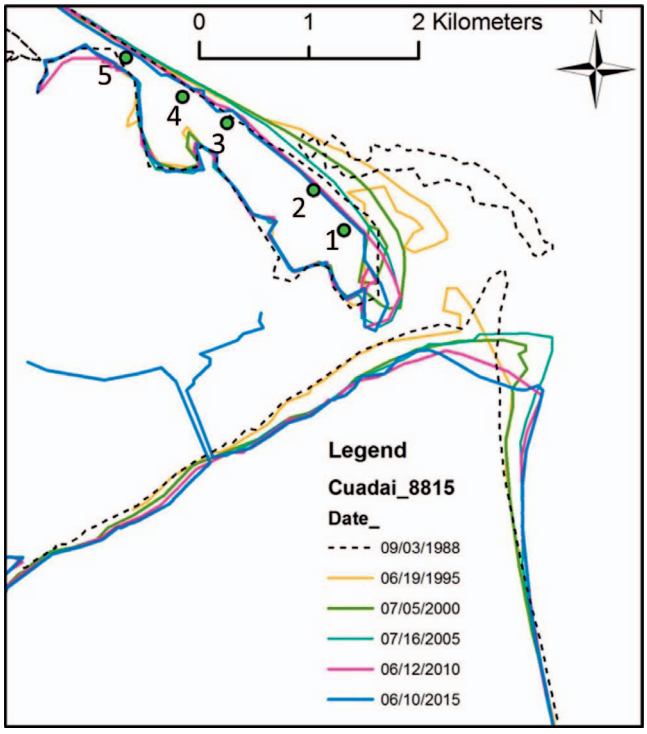

Figure 8. Shoreline positions including the ebb tidal bar welding at Cua Dai Beach from 1988 to 2015 (labels indicate the date of observation, and green dots indicate the location of the first five resorts).

These floods could also have caused the shift of the tip of the south coast in seaward and in the southern direction (Figure 8).

Period 2000–2010

The shoreline change rates for each zone for the period from 2000 to 2010 are shown in Figure 12. The shoreline of the northern coast has continued to erode, with a mean rate of erosion of 12 m/y from 1.5 km to 4.3 km. The erosion has extended to the end of the spit (the yellow bar in Figure 6), with an average rate of 19 m/y from 0.3 km to 1.4 km. In contrast, the southern coast has shown strong accretion. The most accretion at the southern coast is observed from 0.9 km to 3.2 km, with a mean rate of 11 m/y, followed by a gradual decrease in change rates. At the riverbank, an average shoreline retreat of 4.5 m/y is observed over 2.4 km of the shoreline.

The derived volume changes in this period are presented in Table 2. For a closure depth of 5.5 and 7 m respectively, the total sediment loss at the north coast is 323,000 m^3/y to 411,000 m^3/y including zone A and zone D, whereas the southern coast experienced a total gain of 139,000 m^3/y to 177,000 m^3/y. Over this period, the riverbank has experienced a slight erosional pattern of approximately 59,000 m^3/y to 76,000 m^3/y. In terms of total loss, the three zones A, B, and C have lost approximately 104,000 m^3/y to 132,000 m^3/y. The total loss has increased to approximately 243,000 m^3/y to –310,000 m^3/y, including the loss at the spit. Compared with the period 1995–2000 the total loss is less but of the same order of magnitude.

Period 2010–2015

Shoreline change rates of the northern coast, the southern coast, and the riverbank from 2010 to 2015 are shown in Figure 13. The shoreline north of Cua Dai Inlet shows retreat in the order of 6 m/y between 3.2 km and 5.2 km and of 5 m/y from 1.5 km to 3.1 km. A short stretch of shoreline advancement of 4 m/y between 3.1 km to 3.2 km is observed near the location of the Sunrise Resort. The highest erosion is observed over 750 m of the spit, with a rate of 31 m/y. The shoreline south of Cua Dai Inlet indicates accretion. Within the first 850 m south of the inlet, the shoreline advanced an average of 5 m/y. Then the shoreline was stable, with an average accretion of 0.1 m/y over a 2300-m stretch of beach. Erosion and accretion are observed in the riverbank segment, *i.e.* a 1500-m region of retreat with a mean rate of 2.0 m/y and a 750-m region of accretion with average rate of 8.6 m/y.

The volume changes for this 5-year period are presented in Table 2. In general, the northern coast of Cua Dai Inlet shows a negative volume change of approximately 247,000 m^3/y to 315,000 m^3/y for zones A and D. The southern portion is characterized by a positive volume change. The annual volume change in this segment is approximately 25,000 m^3 to 32,000 m^3. The shorelines at the riverbank are characterized by the alternation of erosion and accretion in shoreline change rate but in general the cumulative average volume change shows a positive value of approximately 19,000 m^3/y to 24,000 m^3/y. The whole system lost from 203,000 m^3/y to 259,000 m^3/y, of which major losses have occurred at the northern coast and the spit. In general, the total loss in this period is similar in magnitude to the previous period of 2000 to 2010.

Longshore Sediment Transports

Evaluations of the seasonal and annual longshore transport quantities, S (m^3/y), are carried out on the basis of the CERC formula. The total considered number of days per year is 365 days. The main offshore wave propagation directions and their associated occurring seasons along the year are NE in the winter, ENE in the winter and summer, and SE in the summer. The approximate total considered number of days for each season is summarized in Table 3. The LSTR (m^3/s) in Equation (4) was converted into m^3/y, corresponding to the occurrence probability of each wave direction. To reduce the number of model runs, the average wave periods corresponding to each wave height class have been used to simulate each of the dominant wave directions. The cumulative LSTR corresponding to the summer, the winter, and the annual average are estimated by summary of all LSTR from the waves occurring, as in Table 3. In the following both the results of the wave nearshore transformation and LSRT are presented.

Figure 14 presents examples of the derived nearshore patterns of significant wave heights that are representative for the winter and the summer seasons. For the ENE direction of incident waves, the nearshore wave directions around Cua Dai Inlet show significant influence of diffraction caused by Son Tra Mountain and the Cham Islands group. The significant wave heights behind Cham Islands and in front of the inlet are significantly smaller than for the rest of Cua Dai Beach. In general, the significant wave heights reduce gradually from a deep-water value of 2.3 m to around 0.8 m to 1.2 m in front of

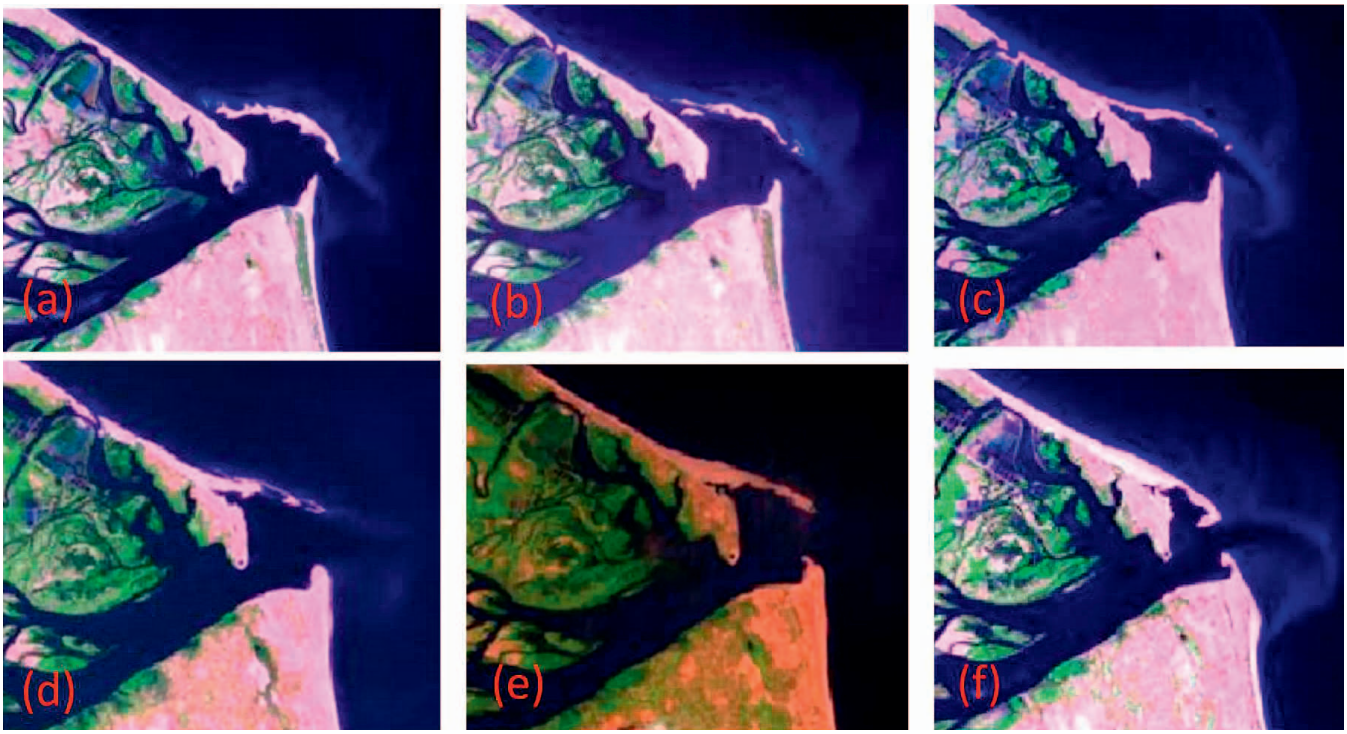

Figure 9. Observed welding of the ebb-tidal delta bar. (a) 3 September 1988; (b) 17 May 1989; (c) 7 July 1990; (d) 10 July 1991; (e) 25 May 1992; and (f) 19 June 1995.

the inlet. For the SE direction of incident waves (Figure 14b), the wave direction of the whole southern coast area is almost SE, except the area behind the Cham Islands and the northern coast of the inlet, where the wave direction turns slightly to ESE. These areas are in the wave shadow region of Cham Islands and of the shoal of Cua Dai Inlet. The results of the nearshore wave transformation during the winter and summer seasons indicate that the northern and southern shorelines of Cua Dai Inlet experience sheltering effects of the Cham Islands in the case of ENE offshore waves. In contrast, only the northern shoreline experiences the impact of the shadow zone caused by waves from the SE.

The LSTR estimated for each wave direction during the summer months and the winter months are indicated in Figures 15 and 16. For the offshore waves from the SE, the LSTR is toward the north on both sides of the inlet (Figures 15c and d). At the northern coast, the LSTR slightly increases from the inlet to the north, whereas at the southern coast the LSTR decreases significantly from the south in the direction of the inlet. The magnitude of LSTR at the southern adjacent coast is larger than at the northern adjacent coast, most likely because the northern adjacent coast is shielded from the SE wave direction by the ebb-tidal delta, reducing the breaking wave height because of diffraction. For the offshore waves from the NE (45° to north), the LSTR is generally toward the southern direction, whereas for the NE waves (60° to north), Figure 16b shows a reversal in the direction of LSTR. Near the inlet, the LSTR is directed to the south, whereas the LSTR is directed to the north farther from the inlet. The LSTR caused by the ENE waves are typical for winter conditions and form the dominant component of the annual longshore transport.

The cumulative LSTR corresponding to the summer season, the winter season, and the annual average are shown in Figure 17. During the summer months, despite the bidirectional occurrence of ENE and SE, the net LSTR is directed toward the north (Figure 17a). At the northern coast, the LSTR increases from the inlet to the north. At the southern coast, the LSTR decreases from the south in the direction of the inlet. For the first 3 km from the inlet toward the north, the LSTR increases from 55,000 m^3/y to approximately 180,000 m^3/y. This positive gradient in LSTR induced by the SE wave would imply erosion of the spit. At the southern coast, the LSTR decreases in the direction of the alongshore transport near the inlet, over a distance ranging from 1.4 km to 4.6 km. This decreasing gradient in LSTR would imply accretion of the first 3 km from the inlet toward the south. On the basis of these derived LSTRs, the longshore sediment transport in the summer would create erosion at the first 3 km at the northern coast and accretion at the southern coast.

During the winter, when ENE events dominate, the LSTR close to the inlet is generally directed to the south. However, there is a transport divergence point at approximately 3 km to the north. A transport convergence point exists at approximately 4 km to the south where the direction of LSTR is toward the north. At the part of the northern shoreline between 3 km to approximately 8 km, the LSTR is toward the north with an average rate of 283,000 m^3/y, whereas near the inlet the LSTR

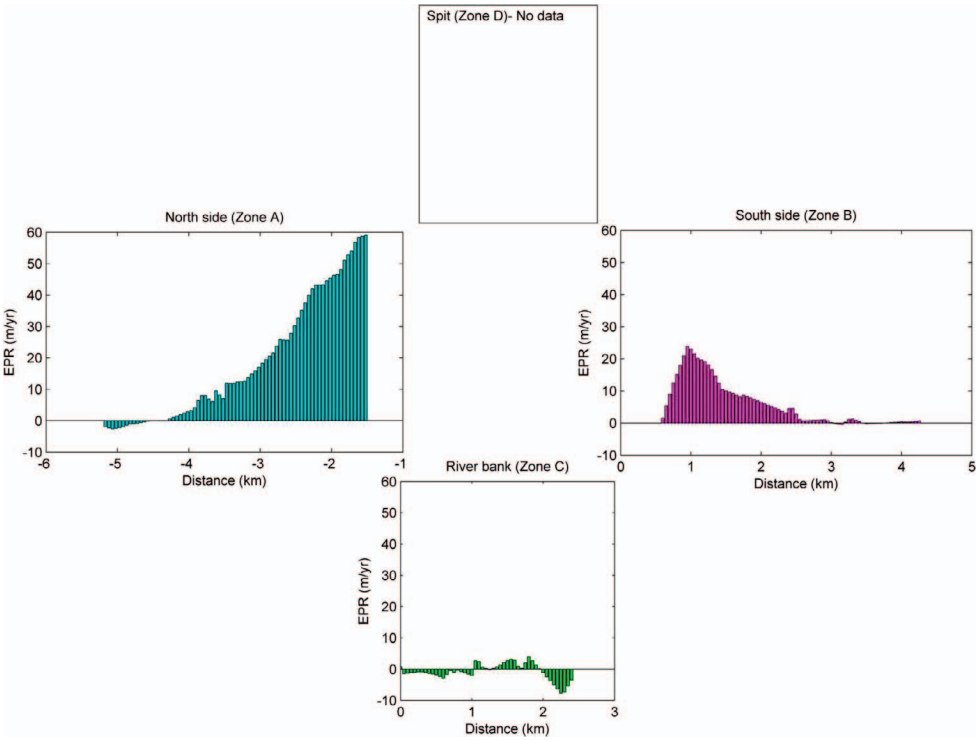

Figure 10. Shoreline change rates from 1988 to 1995. Distance (km) from the inlet measured from the center line of the inlet, with negative values to the north and positive values to the south of the inlet. For the riverbank, distance (km) is positive from the river to the sea. During this period the northern spit did not form; hence, data are absent for this zone. Note that the definition of parameters is given in Figure 6.

is toward the south with an average rate of 87,000 m^3/y. There is a strong gradient from –275,000 m^3/y to 111,000 m^3/y of LSTR at approximately 3 km from the Cua Dai Inlet. This point is near the location of Golden Sand and Sunrise resorts where the shoreline changes orientation. The existence of the transport convergence and divergence locations suggests that local accretion is expected at the southern coast because of a decrease in LSTR, whereas erosion is expected because of an increase in northward transport. Supporting evidence of this is presented in Figures 11 and 12 because the results of volume change during the periods 1995 to 2000 and 2000 to 2010 indicate very strong erosion at the northern and strong accretion at the southern shore. Near the inlet to the north, the longshore sediment transport potential shows a clear decrease, which would result in sand accumulation. However, the results of shoreline change rates and volume change show rapid erosion of the spit. This cannot be explained by the results of gradient in LSTR. This is most likely caused by the presence

Table 2. *Volume changes around Cua Dai Inlet during period 1988 to 2015.* ΔV = the cell volume changes (m^3/yr)

Coastal Zone	A_D (m)	1988–95 ΔV (x10^3; m^3/yr)	1995-2000 ΔV ($\times 10^3$; m^3/y)	2000-10 ΔV ($\times 10^3$; m^3/y)	2010-15 ΔV ($\times 10^3$; m^3/y)
Zone A (m^3/y)	5.5	378	−60	−183	−103
	7	481	−77	−233	−131
Zone B (m^3/y)	5.5	114	−22	139	25
	7	145	−29	177	32
Zone C (m^3/y)	5.5	−10	−335	−59	19
	7	−13	−426	−76	24
Zone D (m^3/y)	5.5			−140	−144
	7			−178	−184
Sum (A + D) (m^3/y)	5.5			−323	−247
	7			−411	−315
Sum (B + C) (m^3/y)	5.5	104	−357	80	44
	7	132	−455	101	56
Sum (A + B + C) (m^3/y)	5.5	481	−418	−104	−59
	7	613	−531	−132	−75
Sum (A + B + C + D) (m^3/y)	5.5			−243	−203
	7			−310	−259

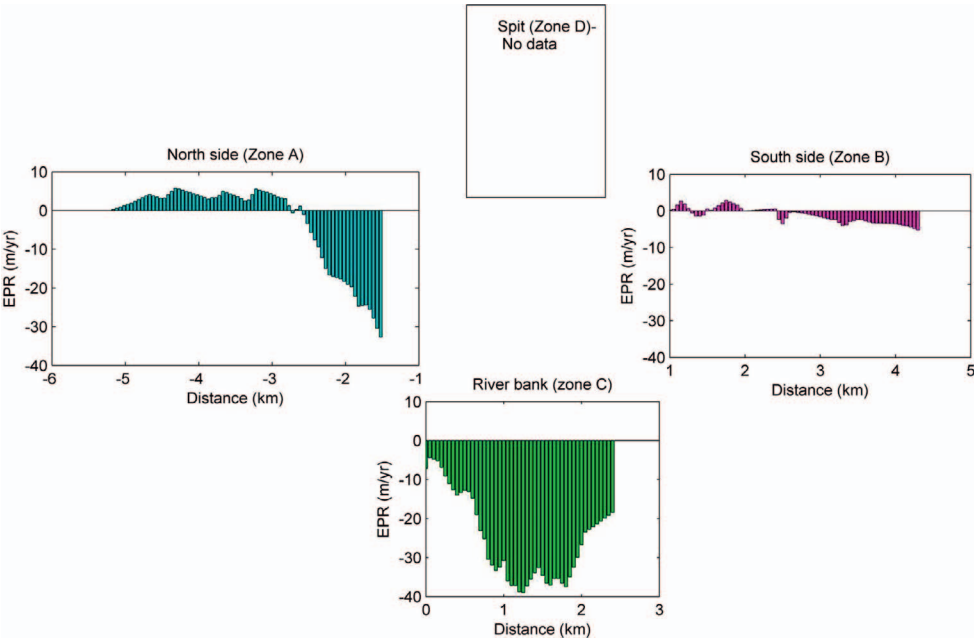

Figure 11. Shoreline change rates from 1995 to 2000.

of resorts and coastal structures and the complex interaction between river regime and tidal regime, which are not taken into account for an LSTR estimation.

The net annual LSTRs are shown in Figure 17c. Generally, the direction of net LSTR is similar to the direction of alongshore transport induced by the waves during the

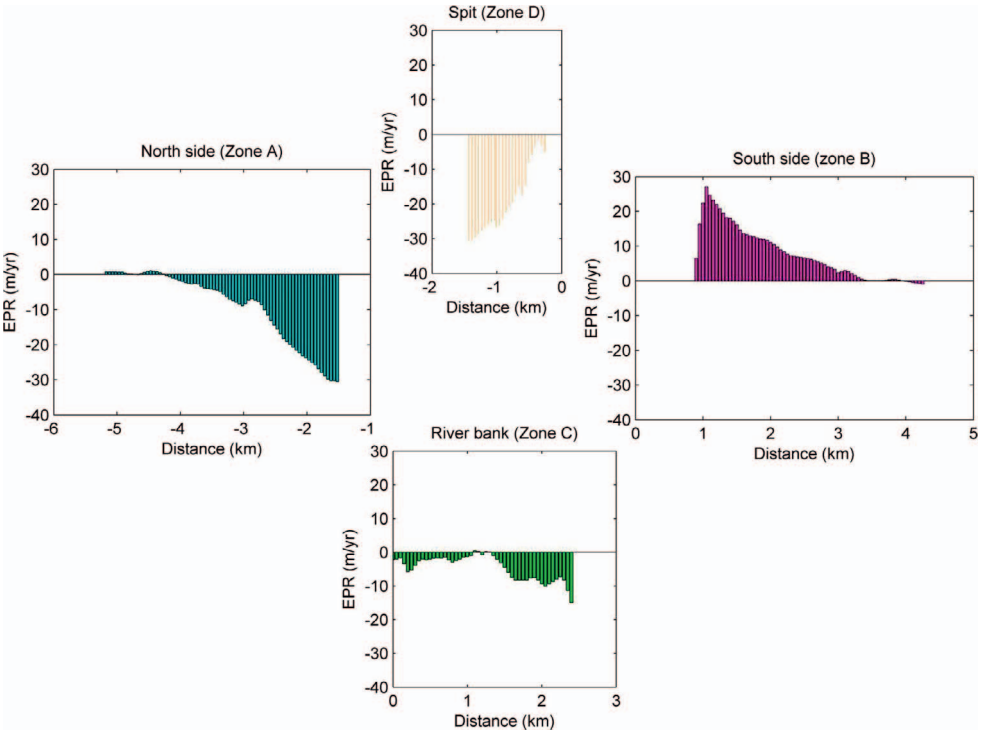

Figure 12. Shoreline change rates from 2000 to 2010.

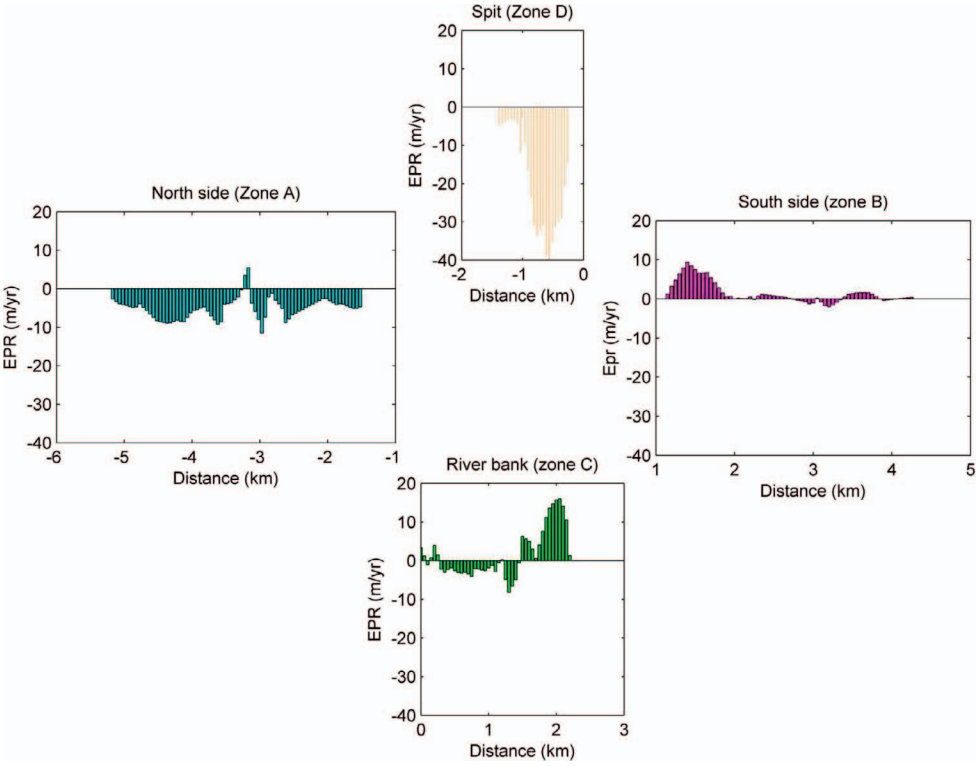

Figure 13. Shoreline change rates from 2010 to 2015.

winter. Waves from the SE contribute to reducing the magnitude of LSTR to the south while enhancing the magnitude of LSTR to the north. At the northern coast the divergence point is still at the same location as present for ENE waves. Approximately 3 km to the north the net transport is oriented toward the north with an average rate of 466,000 m^3/y. From this point southward, the alongshore transport is increasing with a steep gradient from 466,000 m^3/y to almost zero; this suggests intense erosion. Near to the inlet, the LSTR is more or less southward oriented with a relatively low LSTR magnitude. Because from this location the shoreline orientation is changing southward, the sediment transport is found to decrease near the inlet. Especially at the spit the ENE waves compensate the influence of the SE waves, leading to lower magnitudes of the net sediment transport in this area. Close to the inlet at the south side, the waves that come from the ENE are reoriented to the east direction (Figure 14a) because of the impact of shoals of the ebb-tidal delta leading the net LSTR toward the inlet. From this sector the sediment transport is found to decrease toward the convergence point of sediment movement with an average rate of 56,000 m^3/y. From the south segment to the convergence point, the net LSTR is oriented toward the north with an average rate of 526,000 m^3/y. The pattern of net LSTR explains the accretion of the southern coast and erosion of the northern coast.

Table 3. *Wave direction schematizations for the seasonal wind directions used in the longshore sediment transport rate calculations.*

Offshore Wave Propagation Direction	Wave Angle to North (°)	Summer Season (d)	Winter Season (d)
Coming from NE	45		17
Coming from ENE	60	38	139
	75	29	56
Coming from SE	135	44	
	150	42	
Total days		153	212

DISCUSSION

Cua Dai Inlet and its adjacent coasts form a complex system comprising interactions between the ebb-tidal delta, the rivers, their estuaries, and tidal and wave-driven sediment transports. In this section the main mechanisms regarding the extreme erosion problem in this system will be discussed on the basis of the results of observed and calculated shoreline change rate, volume changes, and associated events and human interventions. Even though the erosion problem at Cua Dai receives much attention since 2000, the erosion has been present since 1995 already (Vnexpress, 2014, 2015).

The erosive mode since 1995 was triggered by a long-term geomorphological development of this inlet reflecting a non-periodic cyclic process that takes place over several decades (*cf.* Figure 18). It appears that channel shifting from north to south, triggered by Typhoon Cecil in 1987, caused significant geomorphological changes from 1988 to 2015 to the northern

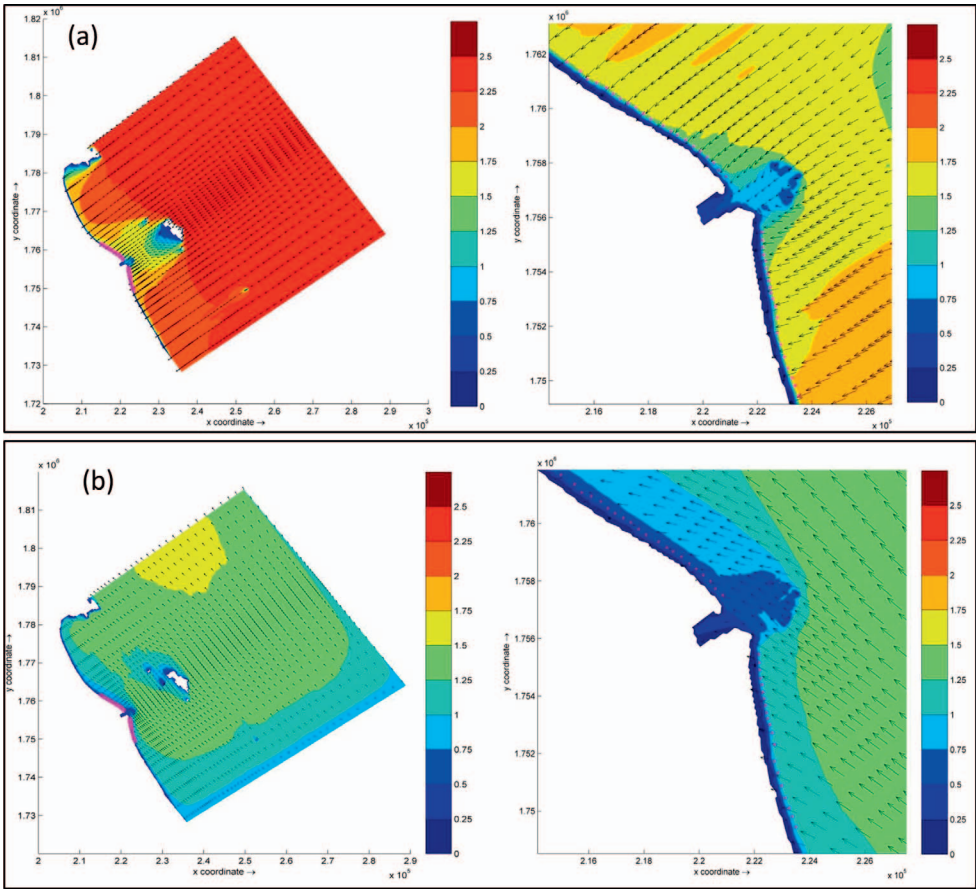

Figure 14. Derived wave fields (winter and summer). (a) Winter season: direction ENE (60°), $H_s = 2.25$ m, $T_p = 7.64$ s; (b) summer season: direction SE (135°), $H_s = 0.75$ m, $T_p = 6.4$ s. The black arrows show the mean wave direction and the colored contour patches indicate the significant wave height. X and Y coordinates indicate the longitude and latitude that convert into the universal transverse Mercator zone 48° N coordination. Pink points indicate the location to extract breaking wave heights.

adjacent coast (Cua Dai Beach) of Cua Dai Inlet. During the first 7-year period, 1988–95, the beach accreted significantly because of the welding of a subareal beach barrier being part of the ebb-tidal delta of Cua Dai Inlet (Figure 9). In general, during this time the system did not experience any impact of human activities but only experienced natural processes. It is hypothesized that the river system provided a large amount of sediment to the inlet gorge or to the ebb-tidal delta, depending on the dry or wet season respectively. Hence, the wave-driven alongshore sediment transport on the northern beaches caused by the ENE waves was available to not only build a shoal such as present in 1988, preventing erosion of the Cua Dai near-inlet shore, but also to feed the more northern shore, annihilating the effect of divergence in transport. Since 1995, after the welding of the ebb-tidal beach barrier, Cua Dai Beach has retreated. The most severe period of erosion is from 2000 to 2010. The average shoreline change rate at the spit was 19 m/y and a mean rate of 12 m/y at Cua Dai Beach. The increasing and northward-shifting erosion rates during that period might be attributed to human causes. At least five resorts and six hydropower dams (Figure 4) were constructed and started to operate and three reclamations were carried out during this period. We hypothesize that the dams and the reclamations have decreased the feeding of the ebb-tidal delta with sediments from the river and its estuary. The impact of the presence of the resorts might be reflected in the results of shoreline change during the next period, 2010–15 (Figure 13). Normally, the LSTR induced by the ENE waves creates a divergence point in the LSRT as indicated in Figure 17b. It means that the sediment source must originate from this coast and the presence of erosion and accretion at the northern coast is expected to be due to the gradients in longshore sediment transport. In the period 2010 to 2015, however, the erosion has been extended farther to the north side of this coast. This is most likely due to the resorts and coastal structures interrupting the wave-driven transport to the north.

The erosion of Cua Dai Beach close to the inlet where the resorts are located is likely also influenced by what is known in the literature as coastal squeeze (Doody, 2004; Gilman, Elison, and Coleman, 2007; Torio and Chmura, 2013) *i.e.* occupying the natural dune area, preventing the natural restoration of a beach and dune area after a storm, promoting erosion. Because

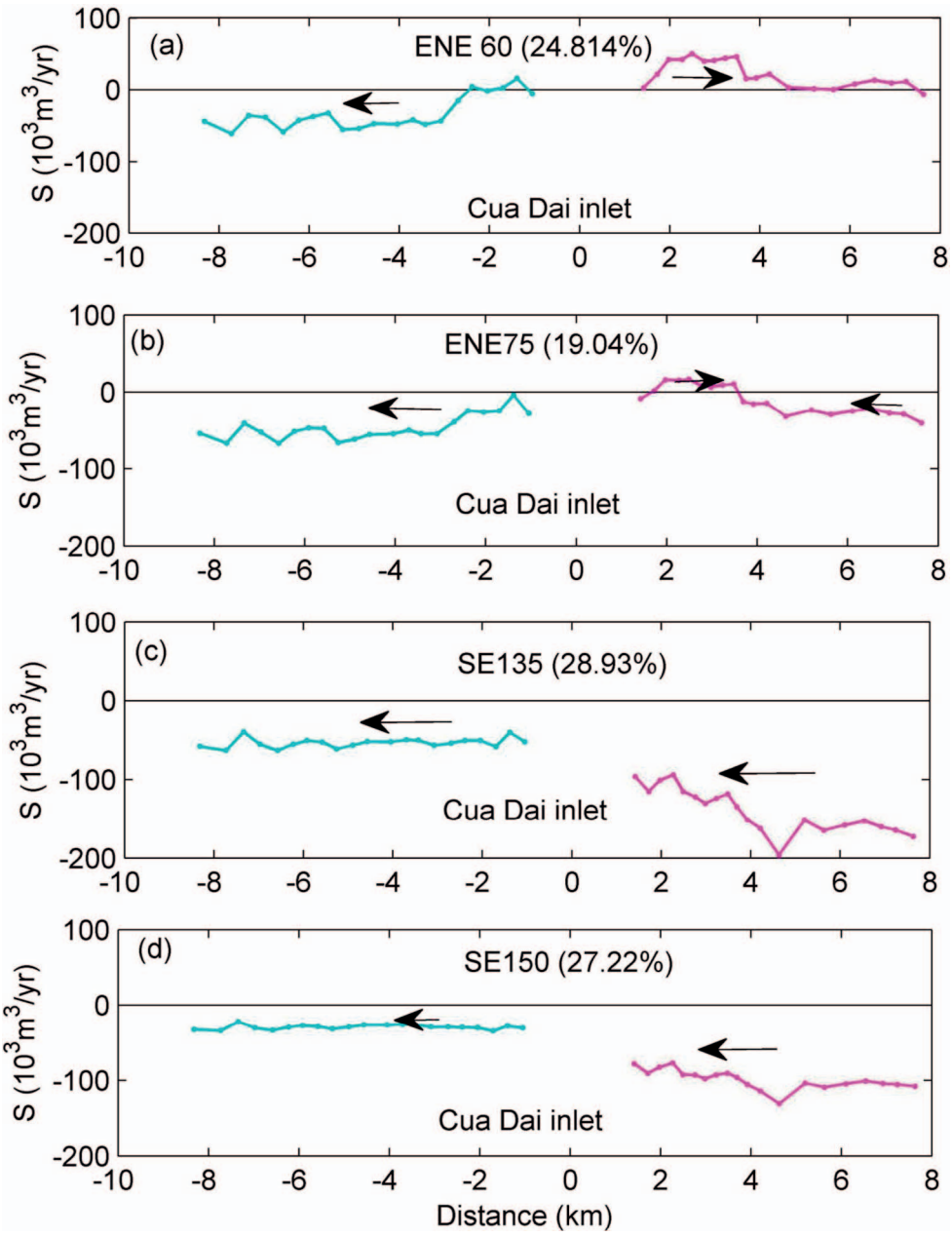

Figure 15. Longshore sediment transport quantities for ENE and SE propagation during the summer. The blue lines indicate LSTR at the northern adjacent coast; the pink lines indicate LSTR at the southern adjacent coast. (Negative indicates northward transport; positive indicates southward transport.) Arrow indicates the direction of LSTR.

the beaches and dunes were originally pristine (no permanent structures), the beach and dune habitats could maintain their integrity by managed retreat (*e.g.*, using tree planting), but with the presence of the resorts and other coastal defense structures this is seriously disturbed. These resorts have caused coastal squeeze in addition to sediment transport blockage toward the updrift side of Cua Dai Beach.

The southern adjacent coast shows signs of a typical downdrift coast that has historically benefited from the bypassing of sediment because of tidal and wave action. During the first period, 1988 to 1995, zone B gained from 114,000 m^3/y to 145,000 m^3/y. From 1995 to 2000 virtually no sediment was gained, whereas it increased again to reach 139,000 m^3/y to 177,000 m^3/y during the next period from 2000 to 2010. It is hypothesized that the sediment input from zones A and C during the flood period (1995–2000) was deposited in the ebb-tidal delta to feed the later accretion of the southern adjacent coast. The amount of sediment receiving at the southern coast

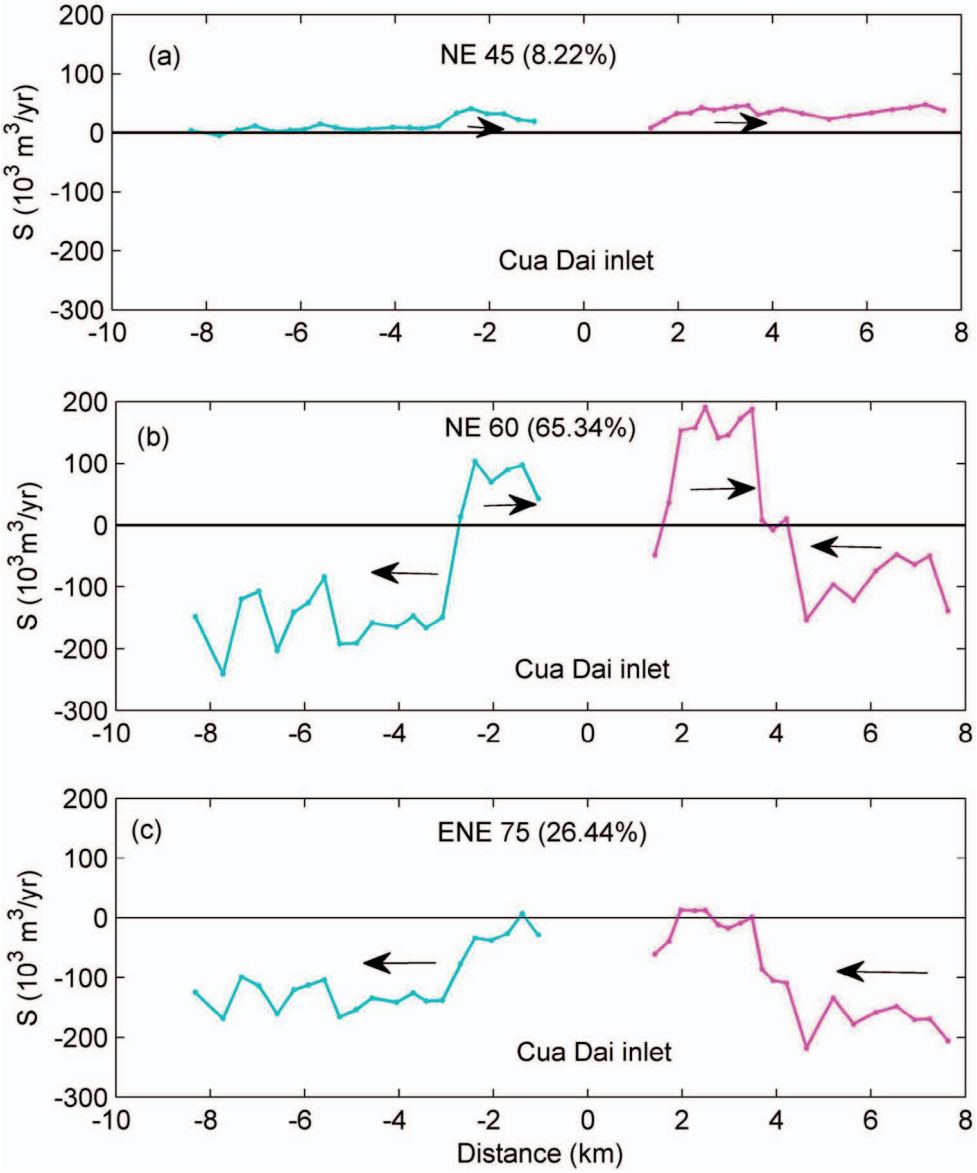

Figure 16. Longshore sediment transport quantities for NE and ENE propagation during the winter. Arrow indicates the direction of LSTR.

has been reduced to 25,000 m^3/y to 32,000 m^3/y during the period 2010 to 2015.

The sediment budgets constructed in accordance with volume changes of the four zones (Table 2) show clear variations. In general, zone A has experienced erosion since 1995, with a total loss of 60,000 m^3/y to 183,000 m^3/y in the period 1995 to 2010, corresponding to 5.5 m of closure depth. The period from 1988 to 1995 is an exception. Because of the occurrence of a welding ebb-tidal bar, zone A accreted with a high amount of 378,000 m^3/y. Since 2000 the northern shoreline has significantly retreated near the inlet (zone D), with a total loss of 140,000 m^3/y to 178,000 m^3/y, corresponding to a closure depth of 5.5 and 7 m, respectively. The adjacent coast to the south of the inlet (zone B) shows historical accretion over the whole 27-year period. Normally sediment gain from bypassing at the southern adjacent coast is approximately 114,000 m^3/y to 145,000 m^3/y, as in the period 1988–95. However, in recent years this amount has been decreased because of reduced sediment availability. In total the system indicates a loss of sediment since 2000 with exception of the first period 1988–95; the system misses some 203,000 m^3/y to 310,000 m^3/y since 2000. The construction of dams in the river system and sediment mining in the estuaries has likely decreased the sediment supply. It is hypothesized that the decrease of the river and estuarine sediment source has triggered erosion along Cua Dai Beach to feed the ebb-tidal delta and the estuarine gorge by wave-driven transport. Instead of being a historical sediment source the gorge and

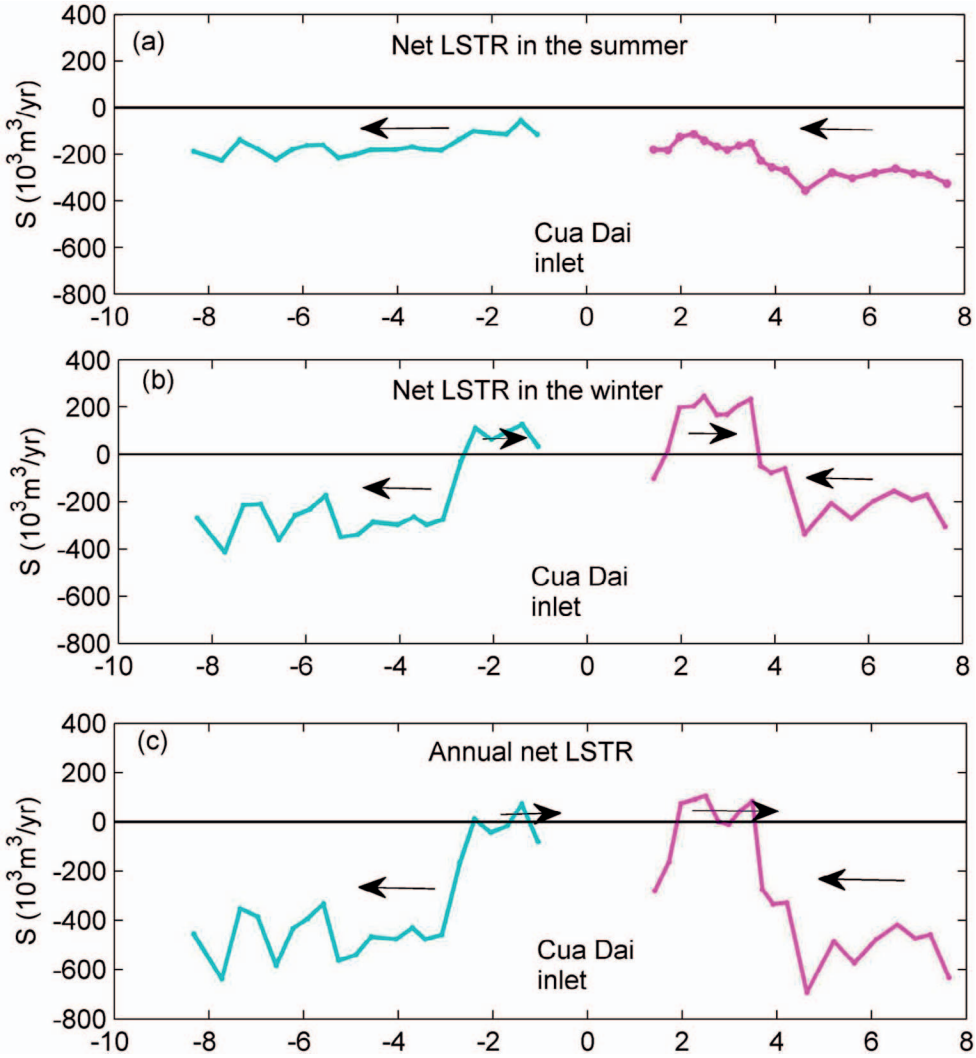

Figure 17. Net longshore sediment transport during the summer (a), the winter (b), and the whole year (c). Arrows indicate the direction of LSTR.

the ebb-tidal delta developed into an important sediment sink that triggered the Cua Dai erosion.

The remaining existence of a bypassing transport system is significantly affected by the seasonal climate, including seasonal waves and seasonal river discharges. A long dry season combines a lower wave-energy condition with a lower river discharge, whereas higher wave energy is associated with a higher flood discharge during the winter season. In the winter/dry season with waves coming from ENE the inlet shoals because of wave-driven sediment transport (Figure 16b) and the lack of significant freshwater discharge to maintain the larger cross-section that was created in the flood season. In the beginning of the rainy typhoon season, flash floods flush out the relatively shallow inlet and the sediment that was deposited in the inlet mouth during the dry period. The flushed sediment is deposited in the ebb-tidal delta. During the winter, waves also induce the alongshore transport and bypass sand to the southern shores. Therefore the amount of sediment bypassing to the south mostly depends on the volume of ebb-tidal delta. The disappearance of the ebb-tidal bar present in 1988 and the huge sediment loss during period 2000 to 2010 indicate that the system lacks sediment at present.

Compared with the observed shoreline change rate, the trends of the alongshore sediment transport show a similar qualitative pattern. Quantitatively, the calculated LSTRs are approximately two times the observed LSTRs, which is quite common in LSTR studies (Bosboom and Stive, 2015). Along approximately 3 km of the northern coast (including zone C and apart from zone A), the net LSTR is increasing with a steep alongshore gradient of 466,000 m^3/y, corresponding to a rate of shoreline change from 24 m/y to 28 m/y, with 5.5 m and 7 m of closure depth respectively. At the same time the observed shoreline change rate at zone A and zone D indicates a rate of 12 m/y and 19 m/y (period 2000 to 2010). Along approximately 4

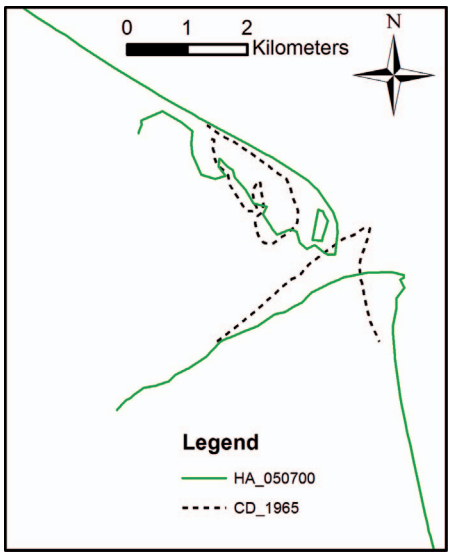

Figure 18. Observed inlet and channel shifting to the south triggered by Typhoon Cecil in 1989. Shoreline in 1965 was taken from Mau (2006).

km of the southern coast, the net LSTR shows a strong decrease from 526,000 m^3/y to almost 56,000 m^3/y. This negative gradient corresponds to approximately 20 m/y to 26 m/y of shoreline change rate, with 5.5 m and 7 m of closure depth respectively. At the same time, the observed shoreline change rate was 11 m/y during the period 2000 to 2010. The probable explanation for these differences lies in the limitations of the CERC formula, both regarding the longshore transport estimation and the neglect of other effects than wave heights and directions alone and of the assumed closure depth.

CONCLUSIONS

Seasonal variations in river discharge and wave climate, human interventions, and the presence of Cham Islands make Cua Dai Inlet a very complex and unique seasonal varying tidal inlet. This study focused on trying to understand the dynamics and evolution of the adjacent coasts of the inlet by a comprehensive investigation of historical shoreline change rates and prevailing wave-driven LSTRs. To investigate the reasons that caused extreme erosion at Cua Dai Beach, this study used remote sensing and GIS techniques to evaluate the shoreline evolution during the period from 1988 to 2015. An empirical approach was applied to estimate the volume changes over four main zones, Cua Dai northern beach (zone A), southern beach (zone B), riverbank (zone C), and spit (zone D, an extended part of Cua Dai Beach). Additionally, the nearshore wave transformation model SWAN was combined with an empirical equation CERC (USACE, 1984) to estimate the LSTR from the dominant offshore wave directions occurring during the summer and the winter seasons and over 1 year.

The analysis indicates that Cua Dai Beach has been eroding since 1995. During the period 1988 to 1995 Cua Dai Inlet was a rich sediment system with a subareal beach barrier being part of the ebb-tidal delta in 1988. During this period, large accretion occurred because of the process of the welding of this barrier to Cua Dai Beach. From 1995 to 2000, Cua Dai Beach eroded at both adjacent coasts of the inlet. Significant erosion occurred during the period from 2000 to 2010, with an average rate of erosion of 12 m/y at Cua Dai Beach and 19 m/y at its southern spit. The southern coast of the inlet experienced strong accretion, with a mean rate of 11 m/y. If we would assume that no sediment is stored in the estuary or ebb-tidal delta, the sediment balance between the northern side, the southern side, and the riverbank indicates that the system has lost a considerable sediment volume. This loss is approximately 243,000 m^3/y to 310,000 m^3/y during the period from 2000 to 2010. At the same time, there are at least seven resorts built close to or even on Cua Dai Beach and seven hydropower plants were constructed upstream of the Vu Gia–Thu Bon River. Besides these activities, illegal sand mining and land reclamation could have contributed to reducing the sediment supply from the river into the Cua Dai Inlet system. These human activities might have created a negative impact on the system in terms of reducing sediment availability contributing to the erosion during this period.

The results from the nearshore wave field modelling indicate that the Cham Islands have an important impact on the offshore wave propagation to the near shore, increasing the complexity of the seasonal wave climate of Cua Dai Beach. Especially in the area around Cua Dai Inlet, waves from the SE induce alongshore sediment transport to the north, whereas the waves from the ENE create LSTR to the south. At Cua Dai Beach, the direction of LSTR shows strong alongshore gradients. At the northern part, predicted transports are directed northward. At the area near the inlet, predicted transport is to the south. There is a large variation in alongshore gradients in LSTR at the northern coast and southern coast, with dominant offshore waves during the winter and the summer seasons. These results contribute to explaining the erosion that occurs at the northern side and the accretion that occurs at the southern coast adjacent to Cua Dai Inlet. The southern coast shows behavior of a typical downdrift-to-an-inlet coast, which has benefited from the bypassing of sediment after the channel switch to the south.

The erosive mode of Cua Dai Beach since 1995 was the result of a long-term geomorphological inlet development reflecting a nonperiodic cyclic process that takes place over several decades. It appears that channel shifting from north to south, triggered by Typhoon Cecil in 1987, dictated the geomorphological development of Cua Dai Beach. The decrease of sediment supply from the river, estuary, and squeeze by coastal developments may have contributed to the erosion. Understanding the role of the ebb-tidal delta as a consequence of channel shifting and its seasonality due to river discharge and wave climate is a remaining challenge.

ACKNOWLEDGMENTS

This study was funded through an Erasmus Mundus Mobility Program with Asia (EMMAsia2014) and supported by Delft University of Technology. The authors gratefully acknowledge the Hydro Meteorological Center in central

Vietnam, and Dr. Tran Thanh Tung, Dr. Mai Van Cong of Thuy Loi University, and Dr. Vo Ngoc Duong of University of Da Nang for providing data for this study. The authors also gratefully acknowledge the excellent reviews by one known reviewer (Dr. L. Benedet) and two unknown reviewers, which greatly improved our manuscript.

LITERATURE CITED

A Vuong Joint Stock Hydropower Company, 2011. http://www.avuong.com/index.php/vi/gioi-thieu-introduction/cong-trinh-nha-may-thuy-dien-a-avuong.html.

Asian Development Bank (ADB), 2014. *VIE: Urban Environment and Climate Change Adaptation Project*. Manila, Philippines: Asian Development Bank, *Document No. IE131001410-06-RP-103,* 134p.

Avinash, K.; Deepika, B., and Jayappa, K.S., 2013. Evolution of spit morphology: A case study using a remote sensing and statistical based approach. *Journal of Coastal Conservation*, 17(3), 327–337.

Avinash, K.; Jayappa, K.S., and Vethamony, P., 2012. Evolution of Swarna estuary and its impact on braided islands and estuarine banks, southwest coast of India. *Environmental Earth Sciences*, 65(3), 835–848.

Bayram, A.; Larson, M., and Hanson, H., 2007. A new formula for the total longshore sediment transport rate. *Coastal Engineering*, 54(9), 700–710.

Bosboom, J. and Stive, M.J.F., 2015. *Coastal Dynamic I: Lecture Notes CIE4305*. Delft, The Netherlands: Delft University of Technology, 573p.

Chander, G.; Markham, B.L., and Helder, D.L., 2009. Summary of current radiometric calibration coefficients for Landsat MSS, TM, ETM+, and EO-1 ALI sensors. *Remote Sensing of Environment*, 113(5), 893–903.

Chen, W.W. and Chang, H.K., 2009. Estimation of shoreline position and change from satellite images considering tidal variation. *Estuarine, Coastal and Shelf Science*, 84(1), 54–60.

Dissanayake, D.M.P.K.; Ranasinghe, R., and Roelvink, J.A., 2012. The morphological response of large tidal inlet/basin systems to relative sea level rise. *Climatic Change*, 113(2), 253–276.

Doody, J.P., 2004. 'Coastal squeeze' – an historical perspective. *Journal of Coastal Conservation*, 10(1), 129–138.

Duong, T.M.; Ranasinghe, R.; Walstra, D., and Roelvink, D., 2016. Assessing climate change impacts on the stability of small tidal inlet systems: Why and how? *Earth-Science Reviews*, 154, 369–380.

Elias, E.P.L. and van der Spek, A.J.F., 2006. Long-term morphodynamic evolution of Texel Inlet and its ebb-tidal delta (The Netherlands). *Marine Geology*, 225(1–4), 5–21.

Gilman, E.; Ellison, J., and Coleman, R., 2007. Assessment of mangrove response to projected relative sea-level rise and recent historical reconstruction of shoreline position. *Environmental Monitoring and Assessment*, 124(1), 105–130.

Gilvear, D.; Tyler, A., and Davids, C., 2004. Detection of estuarine and tidal river hydromorphology using hyper-spectral and LiDAR data: Forth estuary, Scotland. *Estuarine, Coastal and Shelf Science*, 61(3), 379–392.

Hallermeier, R.J., 1978. Uses for a calculated limit depth to beach erosion. *Proceedings of the 16th International Conference on Coastal Engineering* (Hamburg, Germany), pp. 1493–1512.

Hallermeier, R.J., 1981. A profile zonation for seasonal and beaches from wave climate. *Coastal Engineering*, 4, 253–277.

Hapke, C.J.; Lentz, E.E.; Gayes, P.T.; McCoy, C.A.; Hehre, R.; Schwab, W.C., and Williams, S.J., 2010. A review of sediment budget imbalances along Fire Island, New York: Can nearshore geologic framework and patterns of shoreline change explain the deficit? *Journal of Coastal Research*, 26(3), 510–522.

Hayes, M.O., 1979. Barrier island morphology as a function of tidal and wave regime. *In:* Leatherman, S.P. (ed.), *Barrier Islands*. New York: Academic, pp. 1–27.

Ho, L.T.K.; Umitsu, M., and Yamaguchi, Y., 2010. Flood hazard mapping by satellite images and SRTM dem in the Vu Gia–Thu Bon alluvial plain, central Vietnam. *Proceedings of International Archives of the Photogrammetry, Remote Sensing and Spatial Information Science*, 38, 275–280.

Kragtwijk, N.G.; Zitman, T.J.; Stive, M.J.F., and Wang, Z.B., 2004. Morphological response of tidal basins to human interventions. *Coastal Engineering*, 51(3), 207–221.

Lam, N.T., 2009. Hydrodynamics and Morphodynamics of a Seasonally Forced Tidal Inlet System. Delft, The Netherlands: Delft University of Technology, Ph.D. dissertation, 126p.

Maiti, S. and Bhattacharya, A.K., 2009. Shoreline change analysis and its application to prediction: A remote sensing and statistics based approach. *Marine Geology*, 257(1–4), 11–23.

Mau, L.D., 2006. Shoreline changes in and around the ThuBon river mouth, central Vietnam. Goa, India: Goa University, Ph.D. thesis, 162p.

McFeeters, S.K., 1996. The use of the normalized difference water index (NDWI) in the delineation of open water features. *International Journal of Remote Sensing*, 17(7), 1425–1432.

National Weather Service, USA, 2015. http://www.weather.unisys.com/hurricane/index.php.

Nicholls, R.J.; Birkemeier, W.A., and Hallermeier, R.J., 1996. Application of the depth of closure concept. *Proceedings of the 25th International Conference on Coastal Engineering* (Orlando, Florida), pp. 3874–3887.

NOAA (National Oceanic and Atmospheric Administration), 2015. *Wave Watch III*. http://polar.ncep.noaa.gov/waves/.

Oertel, G.F., 1988. Processes of sediment exchange between tidal inlets, ebb tidal delta and barrier islands. *In:* Aubrey, D.G. and Weishar, L. (eds.), *Hydrodynamics and Sediment Dynamics of Tidal Inlets*. New York: Springer, pp. 297–318.

Panda, U.S.; Mohanty, P.K., and Samal, R.N., 2013. Impact of tidal inlet and its geomorphological changes on lagoon environment: A numerical model study. *Estuarine, Coastal and Shelf Science*, 116, 29–40.

Pari, Y.; Ramana Murthy, M.V.; Kumar, S.J.; Subramanian, B.R., and Ramachandran, S., 2008. Morphological changes at Vellar estuary, India – Impact of the December 2004 tsunami. *Journal of Environmental Management*, 89(1), 45–57.

Rajawat, A.S.; Gupta, M.; Acharya, B.C., and Nayak, S., 2007. Impact of new mouth opening on morphology and water quality of the Chilika Lagoon – a study based on Resourcesat-1 LISS-III and AWiFS and IRS-1D LISS-III data. *International Journal of Remote Sensing*, 28(5), 905–923.

Ranasinghe, R.; Duong, T.M.; Uhlenbrook, S.; Roelvink, D., and Stive, M., 2013. Climate-change impact assessment for inlet-interrupted coastlines. *Natural Climate Change*, 3(1), 83–87.

Ranasinghe, R. and Pattiaratchi, C., 1999. The seasonal closure of tidal inlets: Wilson Inlet – A case study. *Coastal Engineering*, 37, 37–56.

Ranasinghe, R.; Pattiaratchi, C., and Masselink, G., 1999. A morphodynamic model to simulate the seasonal closure of tidal inlets. *Coastal Engineering*, 37(1), 1–36.

Rodríguez, E.L. and Dean, R.G., 2009. A sediment budget analysis and management strategy for Port Pierce Inlet, Florida. *Journal of Coastal Research*, 25(4), 870–883.

Rosati, J.D., 2005. Concepts in sediment budgets. *Journal of Coastal Research*, 21(2), 307–322.

Rosati, J.D. and Kraus, N.C., 1999. *Formulation of sediment budgets at inlets*. Vicksburg, Mississippi: U.S. Army Corps of Engineers, *Coastal Engineering Technical Note IV-15,* 20p.

Ruiz de Alegria-Arzaburu, A. and Masselink, G., 2010. Storm response and beach rotation on a gravel beach, Slapton Sands, U.K. *Marine Geology*, 278(1–4), 77–99.

Ryu, J.H.; Kim, C.H.; Lee, Y.K.; Won, J.S.; Chun, S.S., and Lee, S., 2008. Detecting the intertidal morphologic change using satellite data. *Estuarine, Coastal and Shelf Science*, 78(4), 623–632.

Schoonees, J.S. and Theron, A.K., 1996. Improvement of the most accurate longshore transport formula. *Proceedings of the 25th International Conference on Coastal Engineering* (Orlando, Florida), pp. 3652–3665.

Song Ba Joint Stock Company, 2015. http://www.songba.vn/Default.aspx?tabid=fd7219aa-748e-45f5-aa9e-a8820494468b&mid=

dc55835f-ce9e-414e-9540-3f81bcea3929&categoryid=128000513&page=Item.

Song Bung 4 Hydropower Project Management, 2015. http://asb4.vn/index.php/vi/joomla/laster-news.

Stive, M.J.F., 2004. Morphodynamics of Coastal Inlets and Tidal Lagoons. *In*: Klein, A.H.F. (ed.), *Proceedings of the 8th International Coastal Symposium. Journal of Coastal Research,* Special Issue No. 39, pp. 28–34.

Stive, M.J.F.; Tran, T.T., and Nghiem, T.L., 2012. Stable and unstable coastal inlet cross-sectional behaviour. *In:* Kim, N.Q. (ed.), *Proceedings of the Fourth International Conference on Estuaries and Coasts, Volume 2* (Hanoi, Vietnam), pp. 1–12.

Stive, M.J.F.; van de Kreeke, J.; Lam, N.T.; Tung, T.T., and Ranasinghe, R., 2009. Empirical relationships between inlet cross-section and tidal prism: A review. *Proceedings of Coastal Dynamics* (Tokyo, Japan), pp. 1–10.

Stive, M.J.F. and Wang, Z.B., 2003. Morphodynamic modelling of tidal basins and coastal inlets. *In*: Lakhan, V.C. (ed.), *Advances in Coastal Modeling*. Amsterdam: Elsevier, pp. 367–392.

Thieler, E.R.; Himmelstoss, E.A.; Zichichi, J.L., and Ergul, A., 2009. *The Digital Shoreline Analysis System (DSAS) Version 4.0—An ArcGIS Extension for Calculating Shoreline Change*. Woods Hole, Massachusetts: USGS, *Open-File Report 2008-1278*. http://woodshole.er.usgs.gov/project-pages/DSAS/version4/.

Thieler, E.R.; Himmelstoss, E.A.; Zichichi, J.L., and Miller, T.L., 2005. *The Digital Shoreline Analysis System (DSAS) version 3.0, an ArcGIS© Extension for Calculating Historic Shoreline Change*. Woods Hole, Massachusetts: USGS, *Open-File Report 2005-1304*.

Torio, D.D. and Chmura, G.L., 2013. Assessing coastal squeeze of tidal wetlands. *Journal of Coastal Research*, 29(5), 1049–1061.

Tung, T.T., 2011. Morphodynamics of Seasonal Closed Coastal Inlets at the Central Coast of Vietnam. Delft, The Netherlands: Delft University of Technology, Ph.D. dissertation, 166p.

Tuoitre, 2015. *Sand mining along the Vu Gia–Thu Bon River to build up highway project*. http://tuoitre.vn/tin/chinh-tri-xa-hoi/20150807/khoet-song-dap-duong-cao-toc/789846.html.

USACE (U.S. Army Corps of Engineers), 1984. *Shore Protection Manual*, 4th edition. Washington, D.C.: U.S. Government Printing Office, 652pp.

USGS (U.S. Geological Survey), 2017. *Earth Explorer*. http://earthexplorer.usgs.gov/.

Vnexpress, 2014. *Quang Nam has been struggling to resolve erosion problem at Cua Dai beach* (in Vietnamese). http://vnexpress.net/photo/thoi-su/quang-nam-loay-hoay-cuu-bo-bien-cua-dai-3125824.html.

Vnexpress, 2015. *Many resorts along Cua Dai beach have been abandoned by erosion* (in Vietnamese). http://vnexpress.net/photo/thoi-su/nhieu-nha-nghi-ven-bien-cua-dai-bo-hoang-do-sat-lo-3306913.html.